Electrochemistry at Well-Characterized Surfaces

ARTHUR T. HUBBARD

Department of Chemistry, University of Cincinnati, Cincinnati, Ohio 45221

Received July 21, 1987 (Revised Manuscript Received October 23, 1987)

Contents

Arthur T. Hubbard was born in Alameda, CA, in 1941 and was educated in California. He graduated from Westmont College in Santa Barbara, with a bachelors degree magna cum laude in chemistry in 1963. He received his Ph.D. degree in 1967 from the California Institute of Technology, where he held a National Science Foundation fellowship. After graduation he was appointed to the chemistry faculty of the University of Hawaii where he remained until 1976. At that time he was appointed professor of chemistry at the University of California at Santa Barbara. In 1986 he moved to the University of Cincinnati, where he holds an Eminent Scholar endowed chair, a faculty appointment as Professor of Chemistry, and is Director of the Surface Center. Concurrently with his faculty appointment, he is serving as Associate Editor of *Langmuir*, the American Chemical Society journal of surfaces and colloids.

I. Introduction

Low-energy electron diffraction (LEED), first described by Germer and co-workers[1] in experiments that demonstrated the wave–particle duality of matter, began to be recognized as an important tool for surface characterization in 1960 when Germer described results obtained with an improved apparatus[2a] that incorporated the visual display system for electrons developed by Ehrenberg.[2b] The discovery of LEED did more than provide an important technique for investigation of surface structure: LEED captured the imagination of the surface-science community; surfaces could now be examined directly at the atomic level. Efficient, metal ultrahigh vacuum (UHV) systems were developed specifically for experiments with clean surfaces. An extensive complement of other surface investigation techniques followed in rapid succession. Auger spectroscopy and high-resolution electron energy-loss spectroscopy (EELS) are particularly noteworthy.[3] Groups of these techniques were incorporated into one vacuum system, and each technique contributed a share of the information needed to bring the surface to a well-defined state: that is, a state in which the structure and composition of the surface are known at the atomic level from direct experiments. A useful introduction and compilation of references has been provided by Somorjai.[4]

During this same period of time, surface studies by means of thin-layer electrodes revealed that very many of the species adsorbed from solutions at electrode surfaces are covalently bonded to the surface suffi-

0009-2665/88/0788-0633$06.50/0

ciently strongly that they would be expected to remain attached when the surface is transferred from solution to vacuum.[5] All was in readiness for surface electrochemistry to benefit from and contribute to progress in the study of well-defined surfaces at the level of atoms, ions, and molecules. Progress has been rapid as noted in previous reviews.[6,7] Viewed in perspective, this is a potentially large field that is presently at an early stage of its development. Only a few of the virtually unlimited variety of substrates and fluids have been studied, and even those cases are still somewhat fragmentary. The experiments are difficult but becoming easier as a result of refinements in technique. The excitement of this field is growing as the pace of completion of proper experiments quickens and as the various findings begin to fit together to form general principles.[7] It has already become apparent that well-defined surface electrochemistry experiments are important to the growth of understanding in a number of surface-related fundamental scientific areas, such as the surface structure of materials and of solid-liquid interfaces, surface electronic structure and chemical bonding, surface thermodynamics, surface reaction kinetics and mechanisms, surface acid–base chemistry, surface oxidation–reduction processes, surface reaction product distributions, electrical double-layer phenomena, and solvation of surfaces. Numerous practical advances follow from the fundamental developments, due to strong involvement of surface electrochemistry in areas including the behavior of catalysts and electrocatalysts; chemical and clinical analysis based upon electrochemistry; electroplating, etching, or passivation of surfaces; electrochemical synthesis; modification of the surface chemical properties of structural metals, oxides, semiconductors, and polymers; manufacture of electronic microcircuits and detectors; surface phenomena of bones and teeth; and surface-related operations such as lubrication and bonding. In other words, one can safely predict that the best is yet to come.

The objective of this review is to illustrate by examples from the liteature the strengths and limitations of surface electrochemistry done with the multitechnique approach characteristic of investigations involving well-defined surfaces. Only studies at surfaces characterized as to structure and composition or directly traceable to such surfaces are included. Arrangement of the subject matter follows the order in which the mysteries were deciphered, each subsequent result depending for its interpretation on the realizations that preceded it. For this reason the adsorption of electrolytes (including solvents) is considered first, followed by electrodeposition of metals, passivation of surfaces by oxide layers, adsorption of molecules and molecular fragments, and finally the few electrode reactions of well-characterized adsorbed molecules thus far studied.

II. Adsorption from Ionic Solutions

Most of the adsorption studies reported to date employed aqueous solutions. Frankly, most studies would employ water as solvent even if water were not nature's preferred solvent. This is because water is less reactive than other solvents toward the vaguely "noble" surfaces of metals such as Pt, Pd, Cu, Ag, Au, Pb, Bi, and Hg. Furthermore, water is readily freed of surface-active impurities by means of pyrolytic distillation[8] in which steam from ordinary distilled water, mixed with pure oxygen, is passed over a Pt gauze catalyst at 800 °C, followed by further distillation in an ultraclean glass or quartz apparatus to eliminate inorganic pyrolysis products, such as sulfate, perchlorate, phosphate, nitrate, and iodate. For example, the *relative* unreactivity of water toward Pt surfaces is evident both in gas–solid[8] and liquid–solid[9] conditions. Solvents such as alcohols, aldehydes, amides, amines, alkenes, aromatics, sulfoxides, sulfones, and thioethers belong to the most strongly adsorbing category for platinum-group metals. Others such as esters, ketones, ethers, or carboxylic acids are only moderately strongly adsorbed. A few such as alkanes and liquid ammonia are only weakly adsorbed at Pt surfaces. Still others undergo reactions that produce adsorbed products: dimethylformamide (CO), dichloromethane (Cl), or acetone (oligomer). Purification is a major challenge when one works with any of these solvents; the usual commercial forms of these solvents contain significant quantities of surface-active impurities from synthesis, handling, packaging, and/or decomposition during storage. For these reasons work to date has usually employed aqueous electrolytes, although the field has progressed to the point where others can be efficiently studied.

A. Halides

1. Platinum Surfaces in Halide Solutions

Studies have been carried out in which a Pt(111) surface was examined by LEED and Auger spectroscopy following immersion into aqueous KBr or $CaBr_2$ solutions at pH 4, 6, 8, and 10 and electrode potentials in 50-mV increments spanning the full range between the limits imposed by solvent oxidation (O_2) or reduction (H_2).[9] Contrary to the accepted suppositions,[10] Br *atoms* rather than anions are the principal adsorbed form of the halogen. Adsorbed Br atoms undergo reductive desorption at potentials more negative than −0.1 V vs a Ag/AgCl (1 M KCl) reference electrode:

$$\mathrm{Br(adsorbed)} + e^- \rightleftharpoons \mathrm{Br}^- \qquad (1)$$

A sharp, pH-independent voltammetric peak occurs at the onset of Br reductive desorption; LEED studies reveal that this current spike is due to a structural transition within the Br layer:

$$\mathrm{Pt(111)(3\times3)\text{–}Br}\ [\theta_{Br} = {}^4/_9] + xe^- \rightleftharpoons \mathrm{Pt(111)(4\times4)}\ [\theta_{Br} = {}^7/_{16}] + x\mathrm{Br}^- \qquad (2)$$

where x corresponds to only about ${}^4/_9 - {}^7/_{16} = 0.007$ electron/Br^- anion per surface Pt atom, and θ_{Br} is the packing density of Br atoms per surface Pt atom. The Pt(111)(3×3)–Br structure is also formed when Pt(111) is treated with HBr vapor in vacuum.[11] Ordered structures have also been reported when Pt(100) is treated with HBr in vacuum.[11] Br is not strongly adsorbed from alkaline solutions[9] due at least in part to strongly competing adsorption of OH:

$$2\mathrm{Pt} + \mathrm{OH}^- \rightleftharpoons \mathrm{Pt_2OH} + e^- \qquad (3)$$

$$\mathrm{Pt_2OH} + 3\mathrm{OH}^- \rightarrow 2\mathrm{Pt(OH)_2} + 3e^- \qquad (4)$$

That is, the first stage of Pt oxidation retains an ordered Pt substrate surface and a diffuse oxygenous overlayer

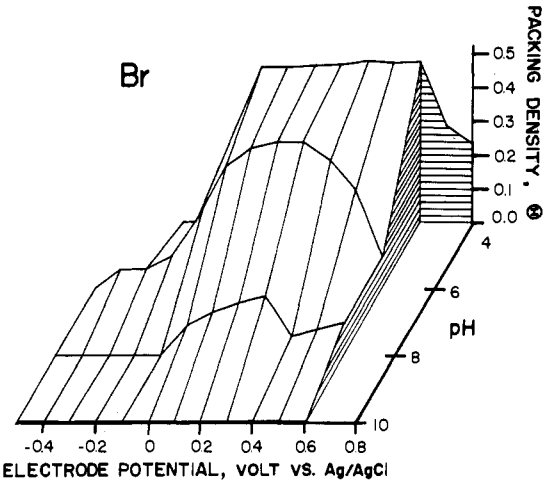

Figure 1. Isometric projection of the adsorption profiles of Br (0.05 mM $CaBr_2$) at Pt(111). Reprinted with permission from ref 9. Copyright 1986 American Chemical Society.

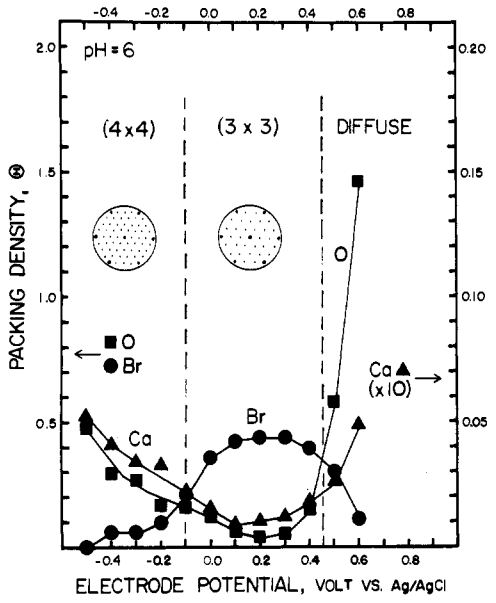

Figure 2. Adsorption profiles of Br, Ca, and O from 0.05 mM $CaBr_2$ (pH 6) at Pt(111) as a function of electrode potential (Ag/AgCl/1 M KCl reference). Reprinted with persmission from ref 9. Copyright 1986 American Chemical Society.

with $\theta_O = 0.5$, whereas in the second stage both the Pt and the O are disordered, $\theta_O = 2.00$. The variation of Br packing density with pH and potential is graphed in Figure 1. Cation packing density, θ_{Ca} or θ_K, goes through a minimum with electrode potential at precisely the point where θ_{Br} is maximum; for instance, at that potential the Ca^{2+} packing density is 30-fold smaller than that of Br (Figure 2). Cation packing density increases somewhat with potentials negative of the Br maximum (probably due to electrostatic attraction) as well as positive of the maximum where surface oxidations also occur. In other words, cation retention is linked to electrostatic effects and adsorbed oxide/hydroxide. When Ca^{2+} ions are present, the surface retains water in vacuum, 5–15 water molecules per Ca^{2+} ion, being largest at alkaline pH. In contrast, K^+ ions, being less strongly hydrated, do not retain detectable amounts of water in vacuum. Due perhaps at least in part to the presence of these traces of adsorbed cations, the Pt surface in bromide solutions is hydrophilic over the entire range of pH and potential.

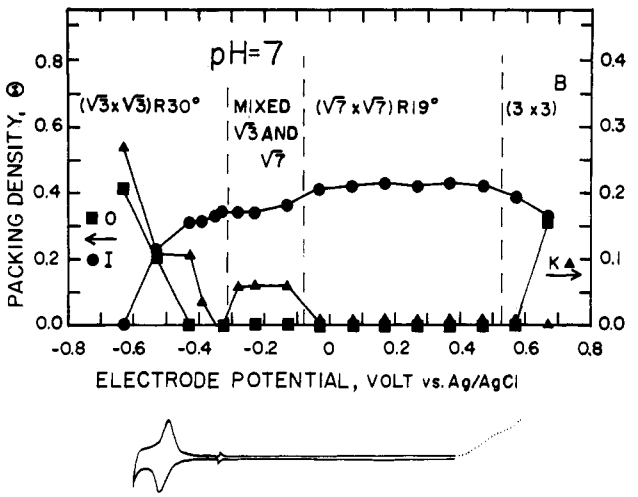

Figure 3. Adsorption profiles of I, K, and O from 0.1 mM KI (pH 7) at Pt(111) as a function of electrode potential (Ag/AgCl/1 M KCl reference). Reprinted with permission from ref 13. Copyright 1987 Elsevier Sequoia.

Adsorption of Br from aqueous Br^- solutions onto a stepped surface, Pt(s)[6(111)×(111)], reveals that Br has no particular affinity for surface steps.[12] Instead, the differences in adsorption behavior between stepped and smooth Pt(111) surfaces are due to formation of different long-range structures in which the terrace width is the characteristic repeat distance, such as Pt(s)[6-(111)×(111)](3×*T*)-Br.[12]

Immersion of Pt(111) into aqueous iodide solutions results in an ordered layer of iodine atoms:

$$KI \rightleftharpoons I(\text{adsorbed}) + K^+ + e^- \qquad (5)$$

Packing density and structure of the iodine atomic layer are potential-dependent (Figure 3). A Pt(111)(3×3)–I [$\theta_I = {}^4/_9$] adlattice is present at moderately positive potentials, a Pt(111)($\sqrt{7}\times\sqrt{7}$)R19°–I [$\theta_I = {}^3/_7$] adlattice in mid-range, and a Pt(111)($\sqrt{3}\times\sqrt{3}$)R30°–I [$\theta_I = {}^1/_3$] adlattice at moderately negative potentials, followed by reductive desorption of I^- anions at the negative extremes of potential. The pH dependence of I adsorption is relatively slight, evidently because adsorption of the halogen is sufficiently strong to suppress adsorption of OH and related oxygen species. A remarkable property of the iodide-treated surfaces is that the Pt(111)(3×3)–I and Pt(111)($\sqrt{7}\times\sqrt{7}$)R19°–I surfaces are hydrophobic whereas the Pt(111)($\sqrt{3}\times\sqrt{3}$)-R30°–I surface is hydrophilic. Transition from (3×3) to $\sqrt{7}$ structure is signalled by a reversible, pH-independent spike in the voltammogram, as well as a change from hydrophobic to hydrophilic behavior. Evidently, an abrupt change in electronic charge density at the interface accompanies the (3×3)-to-$\sqrt{7}$ structural transition. Retentions of K^+ and oxygen species (H_2O, OH, etc.) by the surface are linked but vary oppositely to iodine. The Pt(111)(3×3)–I, Pt(111)($\sqrt{7}\times\sqrt{7}$)-R19°–I and Pt(111)($\sqrt{3}\times\sqrt{3}$)R30°–I adlattices are also observed when Pt(111) is treated with HI or I_2 vapor in vacuum.[13,14] However, the Pt(111)($9\sqrt{3}\times3\sqrt{3}$)-R30°–I structure, which forms when Pt(111) is heated with solid I_2,[15] is not observed to form from aqueous solutions. Adsorption of I_2 vapor onto a stepped Pt surface, Pt(*s*)[6(111)×(111)], reveals no particular affinity of I atoms for step sites of the surface.[16] Instead, the presence of steps results in multiple phase domains

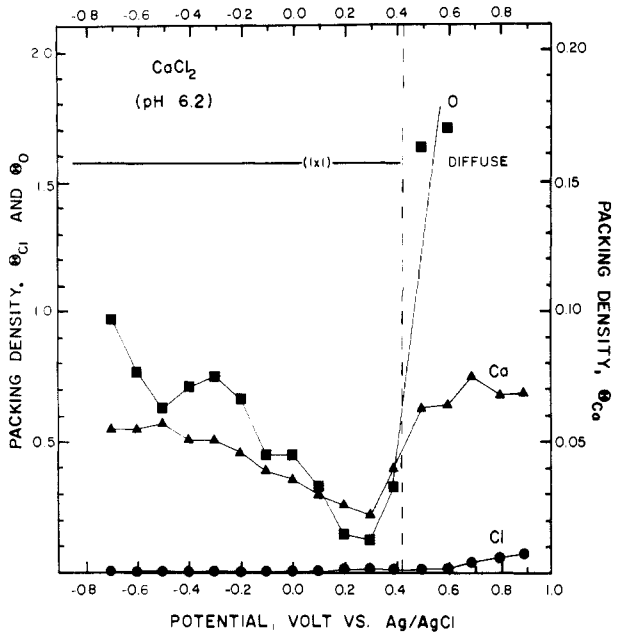

Figure 4. Adsorption profiles of Cl, Ca, and O from 0.05 mM $CaCl_2$ (pH 6.2, 0.1 mM acetate buffer) at Pt(111) as a function of electrode potential (Ag/AgCl/1 M KCl reference). Reprinted with permission from ref 18. Copyright 1987 Elsevier Sequoia.

having (3×3) or ($\sqrt{3}\times\sqrt{3}$)R30° local geometry and structural coincidence of the adjacent terraces: Pt(s)[6(111)×(111)](3×T)–I, Pt(s)[6(111)×(111)](8×T)–I, and Pt(s)[6(111)×(111)](20×2T)–I.[16]

Chemisorption of Cl at Pt(111)[17] is much weaker than that of Br or I, Figure 4. HCl does not form an ordered layer at Pt(111) in vacuum, although it does so at Pt(100).[11] The current due to Cl adsorption/desorption processes was distinguishable from those due to hydrogen adsorption/desorption only because the Cl current is independent of pH:

$$Cl(adsorbed) + e^- \rightleftharpoons Cl^- \quad (6)$$

Only when the HCl concentration exceeds 10 mM is Cl adsorption sufficiently strong to form an ordered layer, Pt(111)(3×3)–Cl [$\theta_{Cl} = 0.33$]. The packing density of Cl is only about half that for an hexagonal close-packed adlattice. Retention of Ca^{2+} by the surface is potential-dependent, with a minimum at about 0.3 V (vs Ag/AgCl), and is twofold larger than that for $CaBr_2$ under comparable conditions. Water is retained by the surface following evacuation to the extent of 6–10 water molecules per Ca^{2+} ion, depending upon the pH. In the absence of strong halide adsorption, the Pt surface is still not "bare" at any electrode potential: the hydrogen adsorption and OH adsorption regions overlap such that the surface contains substantial amounts of one or the other at any potential. Since F is not strongly adsorbed at Pt,[18] a similar domination of the Pt surface by H and OH is to be expected.

2. Silver Surfaces in Halide Solutions

Studies by means of Auger spectroscopy, cyclic voltammetry, and LEED of the surface layers that form when a well-defined Ag(111) surface is immersed into aqueous halide solutions at controlled pH and electrode potential have been reported.[19] If one starts with an oriented single crystal of Ag(111) roughened by gentle polishing with $^1/_4$-μm diamond paste, anodic dissolution

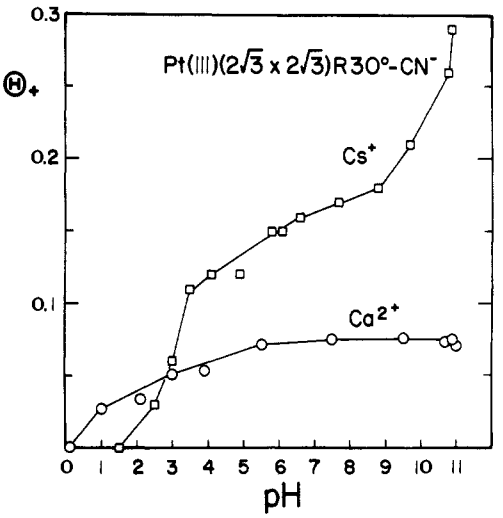

Figure 5. Cation packing density vs pH at Pt(111)(2$\sqrt{3}$×2$\sqrt{3}$)R30°–CN. Experimental conditions: The CN layer was immersed into 0.1 mM Cs^+ or Ca^{2+}; the pH was adjusted by means of HCl, CsOH, or Ca(OH); the electrode potential was 0.1 V (Ag/AgCl/1 M KCl reference). Reprinted with permission from ref 21. Copyright 1985 American Chemical Society.

of Ag produces a surface having the usual hexagonal LEED pattern of Ag(111), although the diffuse scattering intensity in the pattern is noticeably greater than for Ag surfaces prepared by Ar^+ ion bombardment and annealing in UHV. No F adsorption is detectable by Auger spectroscopy. Strong adsorption of Cl, Br, and I occurs throughout most or all of the electrode potential range. Adsorption of these halides at Ag(111) is a redox process as is true for Pt(111):

$$X^- \rightleftharpoons X(adsorbed) + e^- \ (X = Cl, Br, I) \quad (7)$$

Reductive desorption of Cl and Br is nearly complete at the extremely negative potentials near the solvent reduction limit at pH 10. However, iodide remains strongly adsorbed at all potentials studied. The adsorption/desorption process gives rise to a very broad voltammetric feature spanning much of the accessible potential range. Cl and Br form simple Ag(111)($\sqrt{3}\times\sqrt{3}$)R30°–X structures, with $\theta_X = {}^1/_3$, whereas iodide yields some of the same complex structures reported for Ag electrodeposition at iodine-pretreated Pt(111) (see Figure 8B,C). That is, the Ag(111) surface is reconstructed in iodide solutions.

B. Platinum Surfaces in Cyanide and Thiocyanate Solution

Immersion of a well-defined Pt(111) surface into aqueous KCN or KSCN results in formation of an ordered adsorbed layer consisting of chemisorbed species (CNH or CN^-; SCNH or SCN^-) and K^+ counterions, on the basis of LEED following removal from solution.[20] There is a potential-dependent structure of the CN layer: positive of –0.45 V (Ag/AgCl) the adlattice is Pt(111)(2$\sqrt{3}$×2$\sqrt{3}$)R30°–CN [$\theta_{CN} = {}^7/_{12}$]; negative of –0.45 V the adlattice is Pt(111)($\sqrt{13}\times\sqrt{13}$)R14°–CN [$\theta_{CN} = {}^7/_{13}$]. The SCN layer is Pt(111)(2×2)–SCN [$\theta_{SCN} = {}^1/_2$]. Cation packing density at these surfaces is virtually independent of potential, apart from potentials where oxidation of the surface occurred.

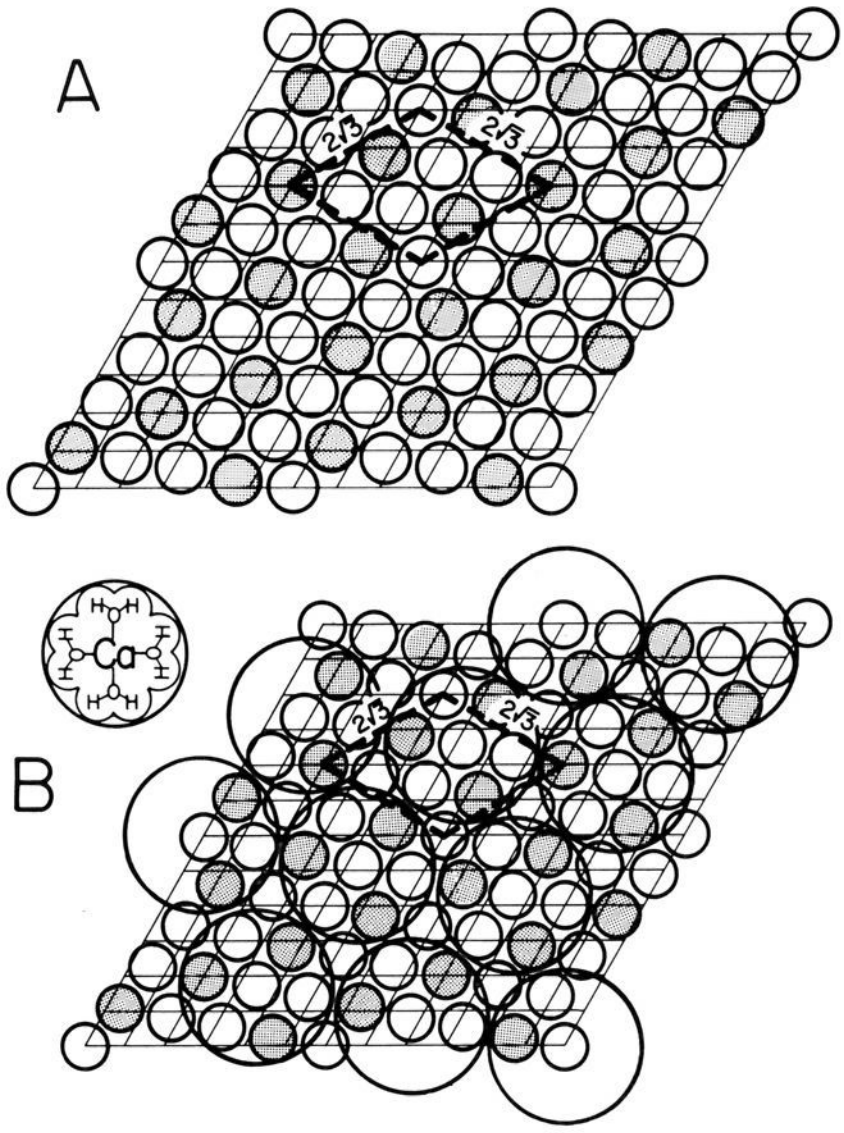

Figure 6. Surface structures. (A) Pt(111)(2√3×2√3)R30°–CN, Cs; (B) Pt(111)(2√3×2√3)R30°–CN, Ca. Shaded circles, CN^- anions; open circles, neutral CNH. Reprinted with permission from ref 21. Copyright 1985 American Chemical Society.

Acid–base behavior of these ordered adsorbed CN and SCN layers was explored by immersion of the coated surface into CsCl or $CaCl_2$ solutions buffered at intervals of about 0.5 pH unit. Such immersion led to replacement of the K^+ ions with Cs^+ or Ca^{2+} without changing the structure of the chemisorbed CN or SCN layer. Measurement by Auger spectroscopy of the amount of Cs present at the surface after immersion revealed that cation retention increases with pH in multiple transitions analogous to a polybasic acid (Figure 5). The first stage of ionization occurs readily as for a strong acid and corresponds in packing density to isolated CN^-Cs^+ ion pairs (Figure 6A).

The final stage of ionization commences above pH 10 and corresponds to formation of adjacent ion pairs. Retention of Ca^{2+} ions commences in a single transition near pH 3 and is limited to only one Ca^{2+} ion per seven adsorbed CN (Figure 5). This is apparently due to the larger size of the hydrated Ca^{2+} ion (Figure 6B). Ca^{2+} remains extensively hydrated even in vacuum.[20] Exactly analogous acid–base behavior is manifested by Pt(111)(2×2)–SCN,[20] even although free hydrothiocyanic acid behaves as a strong acid.

III. Electrodeposition

Composition and structure of electrodeposited layers have been subjects of speculation and indirect experimentation in several thousands of research articles for about 100 years. The long-awaited answers have now been obtained for a few systems, and work is continuing.

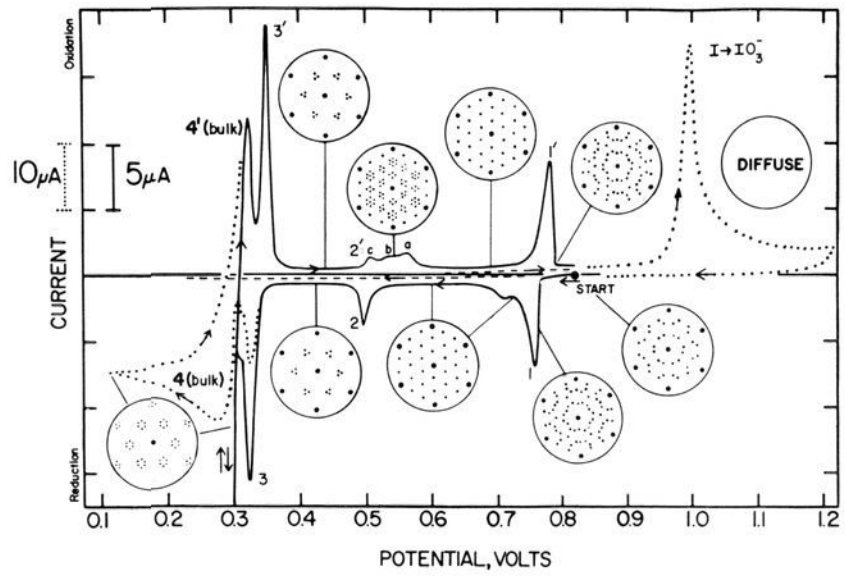

Figure 7. Cyclic voltammogram and LEED patterns. Experimental conditions: 0.1 mM Ag^+ in 1 M $HClO_4$ at the Pt(111)-(√7×√7)R19°–I surface; scan rate, 2 mV/s. Reprinted with permission from ref 22. Copyright 1983 Elsevier Sequoia.

A. Silver Electrodeposition at Platinum Substrates

1. Structure of Electrodeposited Layers

Electrodeposition of Ag onto a well-defined Pt(111) surface has been studied by means of cyclic voltammetry, LEED, Auger spectroscopy, and thermal desorption mass spectroscopy.[21] Prior to electrodeposition the surface was treated with I_2 vapor to form the Pt-(111)(√7×√7)R19°–I adlattice, which protects the Pt and Ag surfaces from attack by the electrolyte and residual gases. The results are illustrated by Figure 7. Electrodeposition of Ag occurs in four distinct ranges of electrode potential: three underpotential deposition processes in which deposition occurs at potentials more positive than the equilibrium potential of the Ag^+/Ag half-cell, followed by electrodeposition of bulk Ag.[22] The iodine layer remains attached to the surface during multiple cycles of electrodeposition/dissolution of Ag: the Auger signal of I does not decrease as the amount of deposited Ag increases (in contrast to the signals due to the Pt substrate);[21,22] the I/Ag signal ratio increases sharply with decreasing angle of incidence of the primary electron beam.[15] Evidently the Ag atoms are able to pass through the iodine layer. LEED patterns observed at various stages of development of the first UPD phase contain all beams of the Pt(111)(√7×√7)R19°–I and Pt(111)(3×3)–Ag,I as noted in Figure 7. This is an indication that electrodeposition forms the Ag monolayer in patches, leaving parts of the √7-iodine layer temporarily unaffected, until finally the (3×3) Ag deposit covers the entire surface. Very close agreement is observed between the amount of Ag electrodeposited and the packing density detected by Ag spectroscopy. LEED patterns observed in connection with the second and third UPD processes contain fractional-index beams clustered near the √3-positions, indicating (√3×√3)R30° local structure, with characteristic splittings of beams indicative of the presence of domains. Combining the LEED, Auger, and voltammetric information with digital simulation of the LEED patterns reveals the specific structural type associated with each stage of the UPD process (Figure 8). The first UPD process forms a (3×3) epitaxial layer of hexagonal

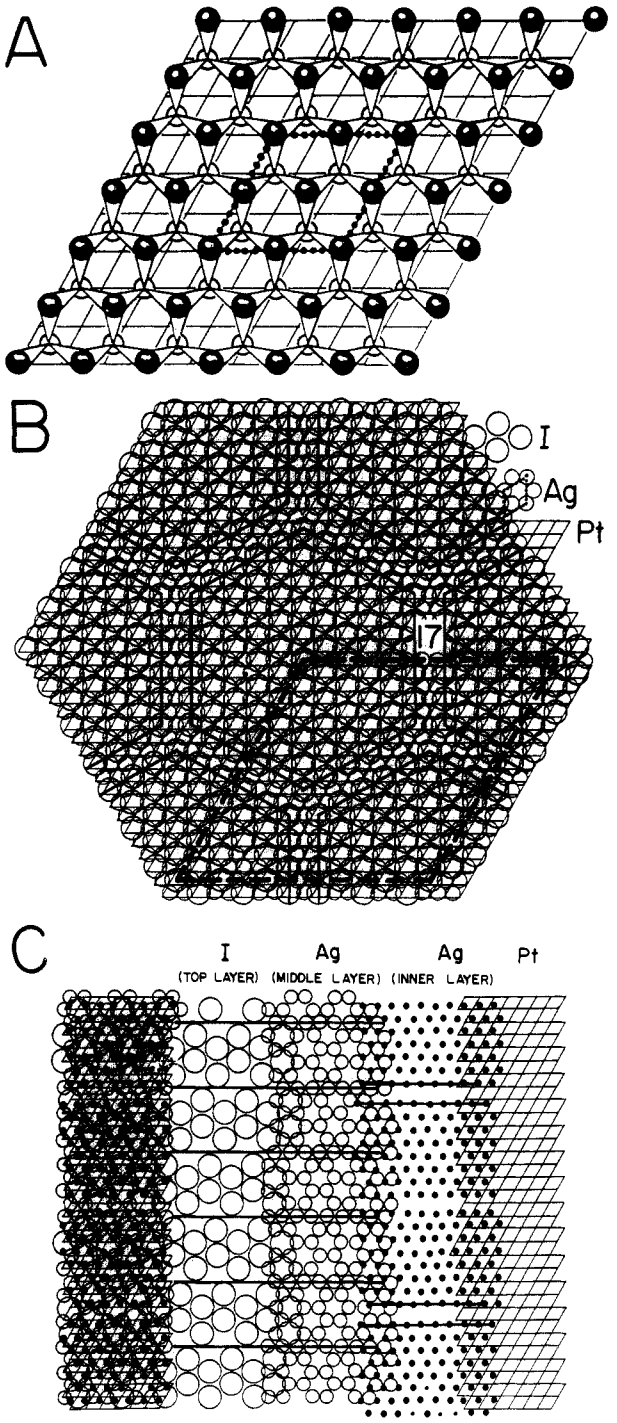

Figure 8. Surface structures of Ag electrodeposited at iodine-pretreated Pt(111). (A) Pt(111)(3×3)-Ag,I, $\theta_{Ag} = \theta_I = {}^4/_9$; (B) Pt(111)($\sqrt{3}\times\sqrt{3}$)R30°-Ag,I with 17-unit domains, $\theta_{Ag} = {}^2/_3$, $\theta_I = {}^1/_3$; (C) Pt(111)($\sqrt{3}\times\sqrt{3}$)R30°-Ag,I with 11-unit (middle layer) and 17-unit (lower layer) domains, $\theta_{Ag} = {}^5/_3$, $\theta_I = {}^1/_3$. Reprinted with permission from ref 16 and 23. Copyright 1983 Elsevier.

close-packed Ag having a layer of iodine atoms adsorbed on top of the layer, resembling the (111) plane of AgI in the usual zinc blend structure. Later stages of UPD produce structures having (3×3)R30° local geometry arranged in domains of sufficiently small width (11–17 Pt unit mesh distances) to give characteristic LEED beams. In the course of LEED studies of electrodeposition it was discovered that the surfaces of oriented Pt single crystals that have been disordered by ion bombardment or electrochemical oxidation and reduction can be restored to a well-defined state by annealing

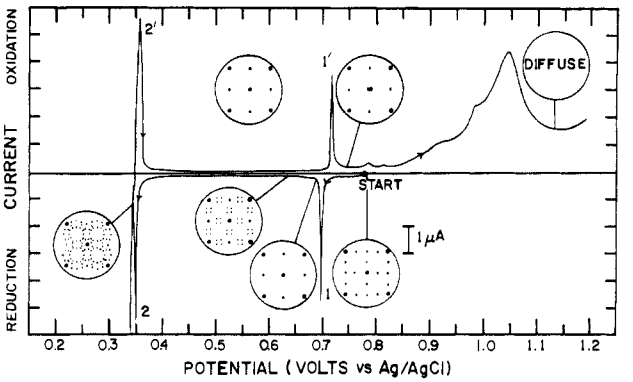

Figure 9. Cyclic voltammogram and LEED patterns for deposition of Ag at the Pt(100) Pt(100)[$c(\sqrt{2}\times\sqrt{8})$]R45°-I adlattice. Experimental conditions: 1.0 mM Ag^+ in 1 M $HClO_4$; scan rate, 2 mV/s. Reprinted with permission from ref 29. Copyright 1984 American Chemical Society.

under an atmosphere of Ar containing I_2 vapor.[15,23] The ordered layer of I atoms is removed quantitatively by subsequent heating in the absence of I_2 to yield an ordered, clean Pt surface. That is, a well-defined Pt surface can be produced by simple procedures not requiring elaborate UHV apparatus, provided the surface damage remaining after metallographic polishing[24] is removed by ion bombardment. It was found that cyclic voltammetry of Ag electrodeposition provides a sensitive and reliable test of surface structure and cleanliness and can be used to monitor surface preparation once the basic UHV experiments to identify the surface structures and demonstrate surface cleanliness of the reference state have been completed.

2. *Influence of Substrate Surface Structure*

Substrate surface structure exerts a powerful influence upon the energetics and structure of monolayer electrodeposition, as illustrated by Figure 9. The UPD process of Ag at I-pretreated Pt(100) occurs in two stages,[23,25] compared with three at Pt(111). The potentials at which UPD occurs and the structures of the deposited layers are different for Pt(111) and Pt(100).

3. *Influence of Adsorbed Layers*

Electrodeposition of metallic monolayers is remarkably sensitive to the nature of the adsorbed layer at the substrate surface: the nature of the adsorbate and the structure or packing density of the adsorbed layer each exert a strong influence. Figure 10 illustrates the influence of iodine layer structure and packing density on UPD of Ag at Pt(100).[24,26] For example, the voltammogram shown in Figure 10B was obtained by a slight variation of the conditions used in Figure 9: The packing density of I atoms was increased by a very small amount (0.02) such that the I layer no longer formed a commensurate structure regularly coincident with the Pt substrate. The effect of this slight change in I packing density and structure was that the Ag electrodeposition process no longer formed a stable, ordered deposit. Although the influences of packing density and structure are difficult to separate, structure appears to be the predominant effect in the present case since the packing-density difference was extremely small. The Pt(100)[$c(5\sqrt{2}\times\sqrt{2})$R45°-I adlattice likewise results in less stable, less well ordered Ag deposits (Figure 10C)

than for Pt(100)(2√2×2)R45°-I (Figure 9); packing-density differences probably are the predominant effect in this case. Slight roughening of the surface by electrochemical oxidation and reduction also has a profound effect on the structure and stability of Ag electrodeposited at Pt[16,24] (Figure 10D) as does surface roughness introduced by Ar^+ ion bombardment (Figure 10E). Similar sensitivity of Ag UPD processes to adsorbed layer structure and packing density was found for Pt(111) surfaces.[16,22,23] Influence of the nature of the adsorbate on metallic monolayer electrodeposition is discussed in the following section.

B. Deposition of Other Metals at Platinum (Cu, Pb, Sn)

Electrodeposition of Cu onto Pt(111) pretreated with I_2 vapor was studied[26] under conditions similar to those described above for deposition of Ag. Electrodeposition of Cu takes place in two narrow, closely spaced UPD potential ranges 0.2 V more positive than bulk Cu deposition. The initial UPD process forms essentially the same (3×3) superlattice as for Ag: Pt(111)(3×3)-Cu,I, for which $\theta_{Cu} = \theta_I = {}^4/_9$ However, the second UPD process yields Pt(111)(10×10)-Cu,I, with $\theta_{Cu} = {}^8/_9$ and $\theta_I = {}^4/_9$. The most striking difference between Cu and Ag deposition at Pt is that electrodeposition of bulk Cu does not occur in the form of monolayers but instead forms separate granules of Cu. The Pt(111)(10×10)-Cu,I surface film is still in evidence by LEED, and the Pt substrate Auger signal remains strong even after deposition of the equivalent of hundreds of monolayers of Cu.

Electrodeposition of Pb onto Pt(111) from solutions containing $PbCl_2$, $CaCl_2$, and HCl reveals ten UPD processes, followed by deposition of bulk Pb.[28] Comparison of Auger spectra (obtained after removal of the surface from solution at various stages during a potential scan) with the coulometric charge for Pb deposition reveals that the Pb deposit is not stable at open circuit in aqueous bromide when the packing density exceeds about $\theta_{Pb} = 1.0$. LEED patterns obtained at various stages during the potential scan demonstrate that the electrodeposited layer is ordered and undergoes a series of structural transitions as Pb is deposited. Adsorbed Cl atoms from the Cl^- electrolyte are present, prior to the onset of Pb deposition, as a Pt(111)(3×3)-Cl adlattice.[18] Cl is present in the topmost layer of the surface at all Pb coverages. Starting with the Pt(111)(3×3)-Cl adlattice, Figure 11A, spontaneous deposition occurs (Figure 11B) followed by electrodeposition of Pb from Cl^- media to produce a series of superlattices: Pt(111)(2 3×2 3)R14°-Pb,Cl in which $\theta_{Pb} = {}^1/_9$ and $\theta_{Cl} = {}^2/_9$ (Figure 11C); Pt(111)(√13×√19)-Pb,Cl, an oblique structure in which $\theta_{Pb} = {}^2/_3$ and $\theta_{Cl} = {}^2/_9$ (Figure 11D); Pt(111)(3×√3split)-Pb,Cl a rectangular structure, $\theta_{Pb} = 0.85$, $\theta_{Cl} = 0.26$ (Figure 11E); and two other rectangular structures, Pt(111)[c(3×5 3)]-PbCl, $\theta_{Pb} = 0.93$, $\theta_{Cl} = {}^1/_3$, and Pt(111)(3×√3)-Pb,Cl, $\theta_{Pb} = {}^4/_3$ and $\theta_{Cl} = {}^1/_3$ (Figure 11F,G). A Pt(111)(2√3×2√3)R30° structure is also found, the stability of which at open circuit is insufficient to permit complete identification. Oblique unit cells such as (√13×√19) (Figure 11D) and rectangular cells such as (3×√3) (Figure 11G) represent a substantial fraction

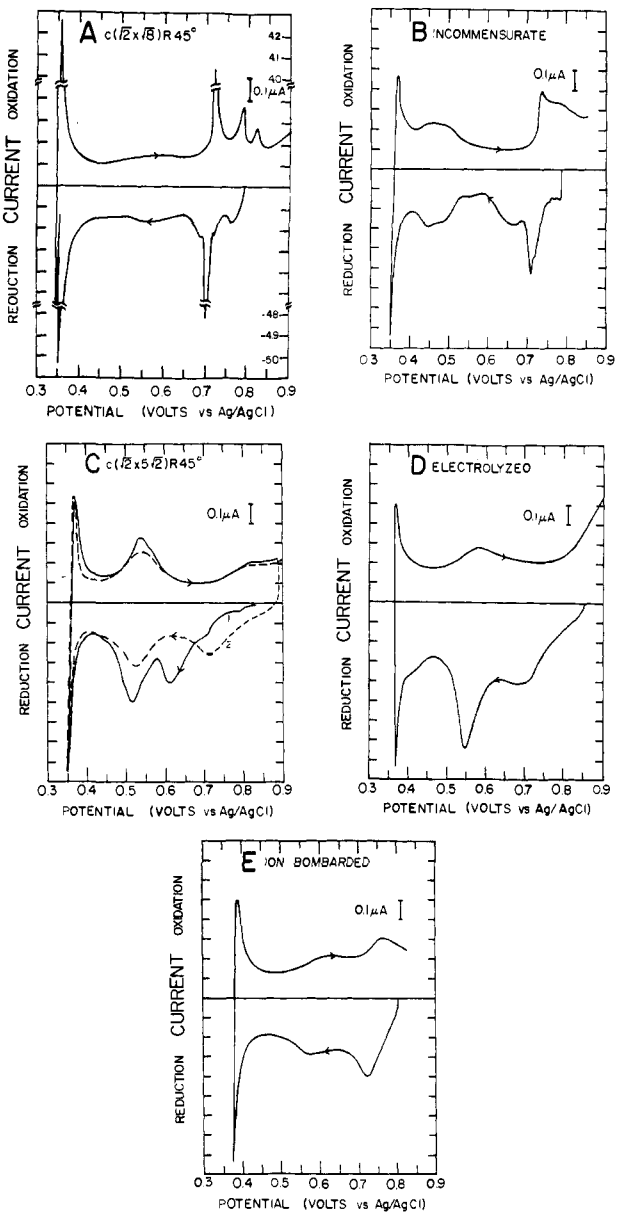

Figure 10. Cyclic voltammograms for deposition of Ag onto iodine-pretreated, (100)-oriented Pt surfaces prepared in various ways: (a) Pt(100)[c(√2×√8)]R45°-I, (B) Pt(100)(1.92√2×√2)R45°-I (incommensurate), (C) Pt(100)[c(5√2×√2)]R45°-I, first (-) and second (--) cycle, (D) Pt(oxidized and reduced)-I, (E) Pt(ion bombardment)-I. Experimental conditions: 1.0 mM Ag^+ in 1 M $HClO_4$; scan rate, 2 mV/s. Reprinted with permission from ref 24. Copyright 1984 American Chemical Society.

of the structures formed in electrodeposition of Pb from various electrolytes.

Electrodeposition of Pb onto Pt(111) from Br^- media likewise forms a lengthy series of ordered UPD superlattices.[30] The Pb deposits are stable only below $\theta_{Pb} = 0.5$ in Br^- media, evidently due to the strong adsorbability of Br at Pt, which destabilizes the Pb deposits. A series of hexagonal and oblique structures are observed by means of LEED as described in ref 30.

Immersion of Pt(111) into a mixture containing 10 mM HBr and 0.1 mM HI at electrode potentials near 0.2 V (vs Ag/AgCl reference) results in a Pt(111)(√7×√7)R19.1°-I adlattice containing no detectable Br.[31] In the absence of HBr the adlattice structure is Pt(111)(3×3)-I.[13] That is, the presence of Br^- ions in the solution influences the structure of the surface layer without being present to a detectable extent in the

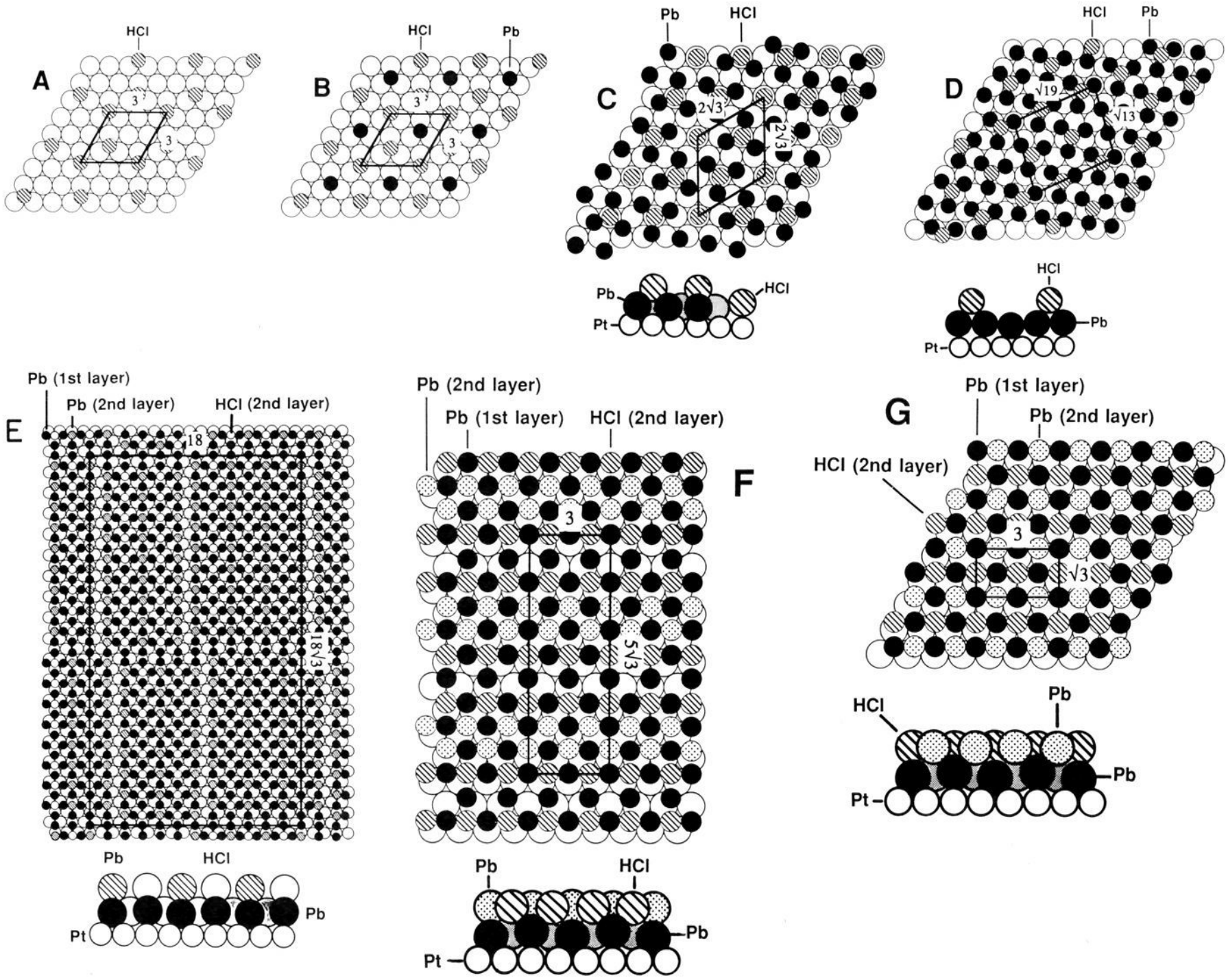

Figure 11. Surface structures of Pb electrodeposited at Pt(111) from Cl^- media. (A) Pt(111)(3×3)–Cl, $\theta_{Cl} = {}^2/_9$; (B) Pt(111)(3×3)–PbCl, $\theta_{Pb} = {}^1/_9$, $\theta_{Cl} = {}^2/_9$; (C) Pt(111)(2√3×√3)R30°–Pb,Cl, $\theta_{Pb} = {}^6/_{12}$, $\theta_{Cl} = {}^2/_9$; (D) Pt(111)(√13×√19)–Pb,Cl, $\theta_{Pb} = {}^2/_3$, $\theta_{Cl} = {}^2/_9$; (E) Pt(111)(3×√3)–Pb,Cl, $\theta_{Pb} = 0.85$, $\theta_{Cl} = 0.26$; (F) Pt(111)[c(5√3×√3)]–Pb,Cl, $\theta_{Pb} = 0.93$, $\theta_{Cl} = {}^1/_3$; (G) Pt(111)(3×√3)–Pb,Cl, $\theta_{Pb} = {}^4/_3$, $\theta_{Cl} = {}^1/_3$. Reprinted with permission from ref 28. Copyright 1986 Elsevier.

chemisorbed layer. Accordingly, electrodeposition of Pb from this Br^-/I^- mixture is analogous to electrodeposition of Ag into the Pt(111)(√7×√7)R19°–I adlattice.[16,22,23] Electrodeposition of Pb under these conditions[31] forms a rectangular Pt(111)(4× 3)–Pb,I superlattice for which the ideal packing densities are $\theta_{Pb} = {}^1/_4$ and $\theta_I = {}^3/_8$ and a hexagonal superlattice, Pt(111)(√13×√13)R14°–Pb,I for which $\theta_{Pb} = {}^7/_{13}$ and $\theta_I = {}^3/_{13}$. Three further UPD processes occur at higher Pb packing densities, but the superlattices lack sufficient open-circuit stability to be fully characterized. Immersion of Pt(111) into solutions containing 10 mM HI and 0.1 mM PbI_2 forms the Pt(111)(3×3)–I[13] adlattice. Electrodeposition of Pb from that solution results in superlattices having relatively limited stability;[31] this result is analogous to electrodeposition of Ag into the Pt(111)(√7×√7)R19°–I and Pt(111)(3×3)–I adlattices.[16]

Immersion of Pt(111) into a solution containing 0.1 mM $SnCl_2$ and an acidic electrolyte such as 10 mM HBr results in the *spontaneous* formation of tin oxides.[32] Anodic electrolysis (oxidation) of the surface increases somewhat the oxidation state of the deposit relative to the spontaneous state, after which the surface becomes passive except for evolution of H_2 at very negative potentials or O_2 at positive extremes. LEED patterns were diffuse, indicating that the tin oxide deposits are disordered. The pathway of spontaneous tin oxide deposition onto Pt appears to be a disproportionation reaction (eq 8) coupled with corrosion of the metallic tin (eq 9). The overall process is shown in eq 10.

$$2Sn^{2+} \rightarrow Sn + Sn^{4+} \quad (8)$$

$$Sn + 2H_2O \rightarrow Sn(OH)_2 + H_2 \quad (9)$$

$$2Sn^{2+} + 2H_2O \rightarrow Sn(OH)_2 + Sn^{4+} + H_2 \quad (10)$$

As recalled in earlier reviews,[6,7] the electrodeposition of hydrogen onto Pt surfaces is a sensitive function of the structure and composition of the surface and also of the nature of the anions present.[32] These findings were confirmed in later work.[33] This work grew out of an earlier study of hydrogen electrodeposition at uncharacterized single-crystal electrodes by Will.[34] Studies involving uncharacterized electrodes require the assumption that the desired surface plane arises from the preparation procedure; further assumptions are required concerning the state of the surface during its use

as an electrode. The problems arising from such assumptions are illustrated by ref 34 in which the undetected surface polycrystallinity led to conclusions contrary to what is presently believed.[32,33] If one reasons by analogy with the results of studies of the electrodeposition of metals onto well-defined surfaces,[16,22-24,26-31] the occurrence of multiple hydrogen-deposition processes on a given single-crystal surface[32] and the dependence of these processes upon the nature of the anions present[9,13,19,21] might be due to formation of various adlattices of H atoms and mixed adlattices of H atoms and species derived from the electrolyte. Unfortunately, the ease of removal of hydrogen from Pt surfaces by evacuation or rinsing complicates the identification of these particular structures.

C. Electrodeposition at Silver Substrates

Electrodeposition of Bi, Pb, Tl, or Cu at the Ag(111) surface[35] involves noticeably smaller underpotentials (energy differences between submonolayer deposition and multilayer deposition) than for deposition of Ag, Pb, or Cu at Pt(111) surfaces.[16,22-24,26-31] Only Bi manifests sufficient stability at open circuit to permit determination of the structure of the electrodeposited layer. The Bi UPD layer electrodeposited from acetate buffer–electrolyte is hexagonal close-packed in a Ag(111)$(2\sqrt{3}\times2\sqrt{3})$R30°–Bi monolayer, $\theta_{Bi} = {}^{7}/_{12}$, in which the $(2\sqrt{3}\times2\sqrt{3})$R30° unit cells are present in strip-shaped domains averaging 8.5 silver unit meshes in width and virtually unlimited length. Electrodeposition of Cu onto Ag(111) gives no UPD peaks. The Cu electrodeposit is stable at open circuit, and consists of a polycrystalline monolayer. On the other hand, electrodeposition of Pb at Ag(111) from acetate, perchlorate, chloride, bromide, or iodide electrolytes, followed by characterization in UHV, yields ordered layers of PbO, the structure of which varies with the nature of the electrolyte anion. Evidently, oxidation of the electrodeposited Pb layer occurs during open-circuit contact with liquid electrolyte just prior to evacuation. Similarly, an electrodeposited monolayer of Tl forms on the ordered TlOH layer during evacuation.

IV. Corrosion and Passivation Studies under Well-Defined Conditions

Studies have been reported of the surface electrochemical behavior of alloy single crystals having a composition (70 atom % Fe, 18 atom % Cr, 12 atom % Ni) resembling that of type-304 stainless steel.[36-39] This alloy has the face-centered cubic close-packed structure in which atoms of the constituent elements are distributed statistically in the fcc lattice positions. Accordingly, X-ray back-reflection photographs of this alloy have the same appearance as for fcc single crystals of pure elements such as Pt, Ag, or Ni. Similarly, the LEED patterns of the clean, annealed FeCrNi(111) surface[38] closely resemble those for Pt(111), Ag(111), or Ni(111). That is, LEED is not element specific. Reconstruction of the FeCrNi(100) surface occurs during annealing in UHV to form a (2×2) structure in which alternate rows of surface atoms are missing.[39] The compositions of the clean (111) and (100) surfaces are virtually the same as the bulk composition.[38,39]

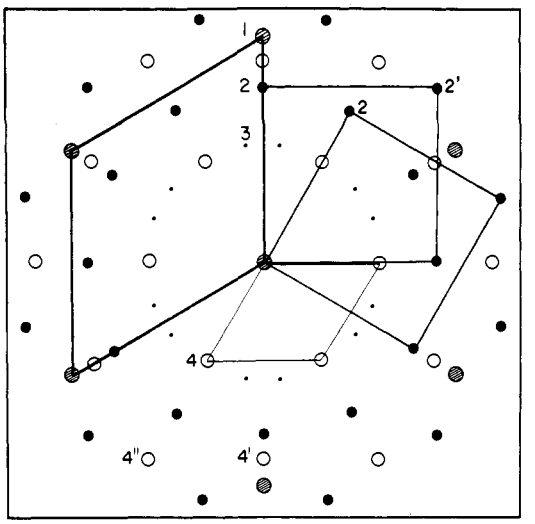

Figure 12. Composite LEED pattern for the FeCrNi(111) surface exposed to electrolytes and annealed. Type 1: integral-index beams due to alloy. Type 2: pattern-of-twelve beams due to square CrO mesh. Type 3: beams due to initial growth phase of oxide with (2×2) local structure in (11×11) domains. Type 4: beams due to Cr_2O_3 (001) film. The alloy contained Fe (70 atom %), Cr (18 atom %), and Ni (12 atom %). Reprinted with permission from ref 38. Copyright 1985 American Chemical Society.

However, heating the surface in the presence of O_2 or H_2O leads to Cr enrichment. Exposure of the alloy surface to water vapor, liquid water, or aqueous solutions at room temperature yields oxide/hydroxide films, which are amorphous and hydrated. Films formed in acidic solutions are enriched in Cr_2O_3 due to selective dissolution of Fe and Cr. Anodic dissolution likewise leads to Cr_2O_3 enrichment of the film. The Auger peaks from 30 to 70 eV due to Fe, Cr, and Ni are shifted with respect to the metallic peaks in a manner expected for surface oxidation.[40-43] Cyclic voltammetry reveals ready passivation of the alloy surface with little current flow in alkaline borate, eventual passivation in H_2SO_4 or $HClO_4$ offer an active–passive transition involving relatively high current, and only partial loss of activity after a transition at high current in HCl.[38] When the amorphous oxide film formed in water vapor, liquid water, or any of the electrolytes studied is heated in vacuum, water is evolved from the surface in separate processes at 300 and 700 °C. Reduction of iron and nickel oxides by chromium occurs during heating to give an oxide layer of nearly pure Cr_2O_3. The annealed oxide is highly ordered. The FeCrNi(111) oxide LEED patterns are summarized in Figure 12. The integral-index beams, type 1 in Figure 12, are not seen for the oxide film, indicating that the film is continuous and of thickness often greater than atomic layers (thicknesses of 25 Å are typical). Beams indicative of an hexagonal superlattice with lattice constant 4.9 Å rotated 30° with respect to the unit mesh of the clean FeCrNi(111) surface (type 4 of Figure 12) are present. These are the correct dimensions for the (001) plane of Cr_2O_3, oriented with the 0–0 vectors parallel to the interatomic vectors of the alloy. Also present is a pattern-of-twelve, consisting of three domain types of a square mesh, type 2 in Figure 12. These type-2 beams are associated with emergence of the integral-index beams and are therefore associated with thin regions of the oxide film. Beams of type 3, due to (11×11) domains of (2×2) local

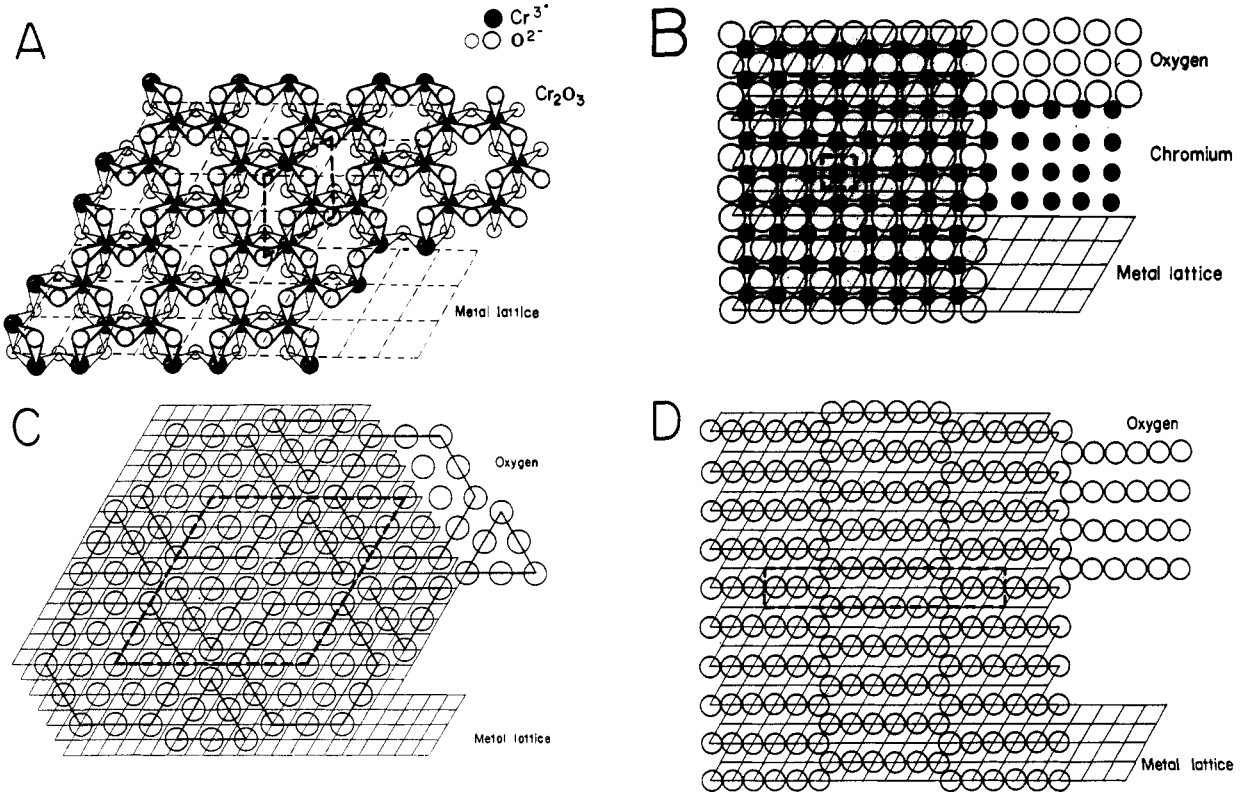

Figure 13. Surface structures at FeCrNi(111). (A) (001) plane of the Cr_2O_3 structure situated on the alloy substrate as experimentally determined. (For clarity, only a few layers of the oxide are shown.), (B) Square CrO structure, (C) Growth phase structure (11×11), (D) Alternative growth phase structure (11×√3). Reprinted with permission from ref 38. Copyright 1985 American Chemical Society.

structure, are present only during early stages of film growth, such as after heating of the clean surface with water vapor in vacuum or after treatment of the surface with HCl solutions. Structure consistent with the LEED patterns, composition, and chemical properties of the film are shown in Figure 13. Reimmersion of the annealed oxide film into electrolyte solutions leads to the important finding that the Cr_2O_3 film (type-4 beams) is stable in solution, whereas the CrO mesh (type-2 beams) vanish on contact with $HClO_4$, H_2SO_4, or HCl, and the Fe Auger signals increase. Evidently, acidic electrolytes, especially HCl, attack the ordered oxide film at the comparatively thin CrO regions, replacing these regions with a thin, hydrated amorphous iron oxide layer. The FeCrNi(100) surface likewise forms the Cr_2O_3(001) oxide film upon being annealed during or after exposure to aqueous media.[39] Square CrO structures are observed for FeCrNi(100) analogous to but differing slightly in structure from those of FeCrNi(111).

Study of corrosion and passivation phenomena under well-defined conditions, as yet in a preliminary stage, illustrate the principal that the same advantages of definitiveness and generality that make this multitechnique approach the path of choice for the study of relatively simple "academic" samples should be even more advantageous when one deals with the more complicated "industrial" samples.

V. Molecular Adsorption

Recent breakthroughs in surface chemistry and electrochemistry have made it possible to characterize molecular adsorption at electrode surfaces to a degree that was not previously possible. Availability of electrode surfaces, the structure and composition of which are known and reproducible, has set the stage for definitive experiments and sophisticated practical applications.[6] That such surfaces can be produced at ambient pressure with simple apparatus[16,24] is all the more encouraging. Auger spectroscopy has been brought to the point of usefulness for monitoring electrode-surface cleanliness and for determination of adsorption isotherms at electrode surfaces.[9,13,18,35] Since all elements except H and He are measurable, Auger spectroscopy has set aside the earlier limitation that electroanalytical methods are applicable only to substances having distinguishable electrochemical activity. LEED serves as a convenient probe of substrate surface and overlayer structure.[9,22] Electron energy-loss spectroscopy (EELS) has recently begun to yield vibrational spectra of remarkable usefulness for organic molecules adsorbed at well-defined electrode surfaces.[44-47] Reflection adsorption infrared spectroscopy has been applied to well-defined surfaces in UHV,[48] and its application to well-defined electrode surfaces is expected soon. The initial results are encouraging: molecular species interact with well-defined surfaces in a relatively straightforward manner; clear correlations between adsorbed states and electrochemical reactivity are beginning to emerge. A wide range of applications of well-defined electrode surfaces is expected because procedures for surface characterization can be of assistance in the study of any solid–liquid interface, and in general no limitations need be imposed upon the electrochemical side of the investigation.

A. Adsorption at Polycrystalline Pt Thin-Layer Electrodes

Investigation of adsorption processes at electrode surfaces and electrode reactions of adsorbed molecules with the aid of thin-layer electrodes,[5] in which the solution under investigation is confined in a thin film (20-μm thickness) near the electrode surface, offers advantages over other electrode designs: surface cleanliness is easier to maintain because only a tiny volume of liquid contacts the electrode surface in each experiment (about 4 $\mu L/cm^2$ of electrode area), surface-adsorbed material constitutes a relatively large proportion of the total material involved in an experiment because of the relatively large area-to-volume ratio of the thin layer of solution, and the task of theoretically describing the adsorption processes and the chemical/electrochemical reactions of the adsorbed layer is much simpler than usual because mass transport considerations are eliminated from the governing equations by proper choice of experimental conditions.[49] Of course, thin-layer electrodes also have some limitations for adsorption studies: in general, only adsorbates displaying electrochemical reactivity that is readily distinguishable from background reactions of the electrode and electrolyte can be efficiently studied, and precision thin-layer electrodes are not conveniently adaptable to surface-characterization experiments in UHV. In view of these advantages and limitations, thin-layer electrodes have been employed for initial explorations of surface adsorption and electrocatalysis processes involving distinctly electroactive substances, followed later by more definitive experiments involving electrochemical methods assisted by surface diffraction and spectroscopic methods.

More than 50 compounds related to hydroquinone have been studied with respect to adsorption at polycrystalline Pt thin-layer electrodes because the reversible quinone–diphenol couples are well-suited to adsorption measurements by TLE (eq 11) and the results

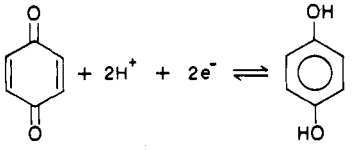

(11)

are revealing a number of important aspects of molecular adsorption at electrode surfaces and of the reactions undergone by adsorbed layers. Electrochemical reactivities of adsorbed and unadsorbed forms of this large family of compounds are very different, as indicated by Figure 14. Electrolysis of the unadsorbed material occurs at less positive potentials than (and completely separately from) oxidation of the adsorbed material. This separability of adsorbed and unadsorbed reactivity is useful for measurement of packing density (mol/cm^2) as follows:[51] when one works with very dilute solutions of strongly adsorbing compounds, it is necessary to fill the thin-layer cavity with surfactant repeatedly in order to satisfy the adsorptive demands of the surface. If during the first filling all of the solute is taken up by the electrode surface, solute peaks will be absent from the subsequent voltammetric scan. In that case the amount of material taken up during the first filling, Γ_1 (mol/cm^2) can be calculated from eq 12,

$$\Gamma_1 = VC^\circ/A \tag{12}$$

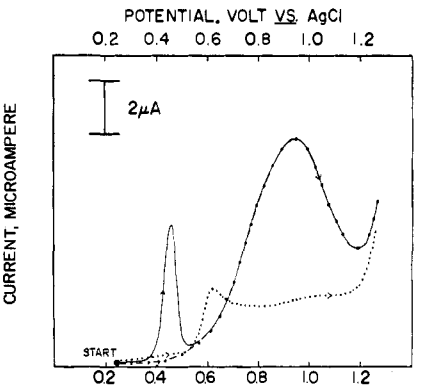

Figure 14. Thin-layer current–potential curves for hydroquinone (HQ) at a polycrystalline Pt electrode: solid curve (–), HQ solution at presaturated surface; broken curve (- - -), presaturated surface rinsed to remove unadsorbed HQ; dotted curve (···), clean surface in pure electrolyte. Experimental conditions: electrolyte was 1 M $HClO_4$; HQ concentration, 0.15 mM; thin-layer volume, 4.08 μL; electrode area, 1.18 cm^2; potential sweep rate, 2 mV/s; temperature, 296 K. Reprinted with permission from ref. 50. Copyright 1982 American Chemical Society.

where V = thin-layer cell volume, C° = initial adsorbate concentration (mol/cm^3), and A = real electrode area (cm^2). If a number of fillings, k, is required to build up the adsorbed layer then the total amount adsorbed at that stage is

$$\Gamma_1 + \Gamma_2 + \ldots + \Gamma_k = kVC^\circ/A \tag{13}$$

The next filling ($k + 1$) leads to a dissolved excess of surfactant detected by means of thin-layer voltammetry and quantitated with the aid of thin-layer coulometry, Q (coulombs). The adsorbed amount is found from the dissolved excess by the Faraday law:

$$\Gamma_{k+1} = (Q_{k+2} - Q_{k+1})/(nFA) \tag{14}$$

where n = number of Faradays per mole electrolyzed, and F = Faraday's constant. The final ($k + 2$) filling leads to no further adsorption and is used to determine the bulk solute concentration, C°:

$$C^\circ = (Q_{k+2} - Q_b)/(nFV) \tag{15}$$

where Q_b = coulometric charge due to background reactions occurring under conditions identical with ($k + 2$) except that dissolved surfactant has been rinsed from the thin-layer cavity with pure electrolyte. The final interfacial concentration is the sum, Γ, of ($k + 1$) components, Γ_j:

$$\Gamma = \sum_{j=1}^{k+1} \Gamma_j \tag{16}$$

A few of the adsorbed compounds display reversible electrochemical reactivity at the same potentials where unadsorbed species react. One determines the amount of this adsorbed electroactive material by rinsing the TLE with surfactant solutions and then with pure electrolyte, followed by coulometry.

1. Influence of Adsorbate Concentration

Packing densities ($nmol/cm^2$) measured as described above for 28 compounds at polycrystalline Pt electrodes as a function of adsorbate concentration are shown in Figure 15. Adsorbate packing-density plateaus accurately measured at smooth, uncontaminated surfaces correlate completely consistently with adsorbate mo-

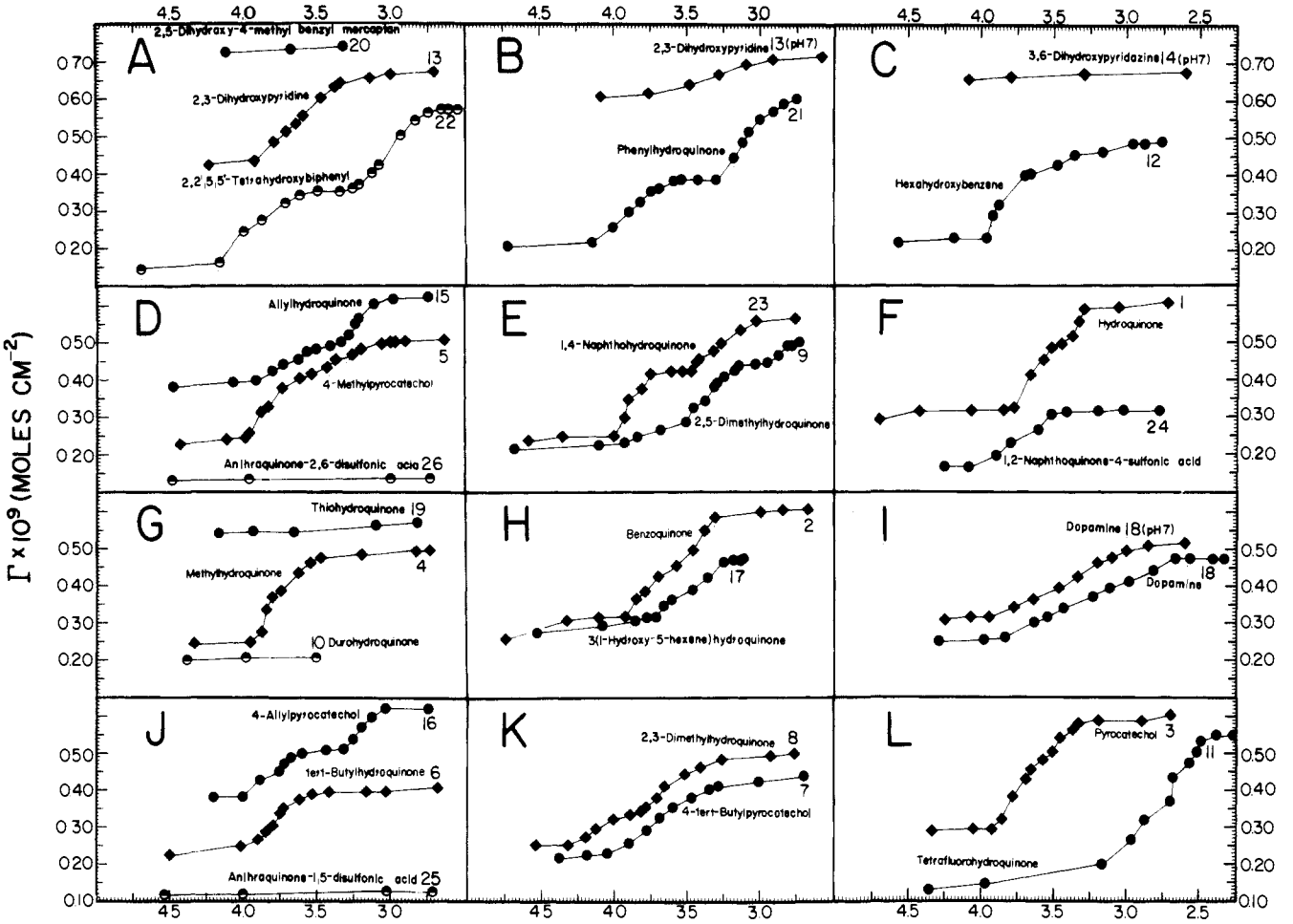

Figure 15. Packing density, Γ (mol/cm²), vs adsorbate concentration (mol/L) at a polycrystalline Pt thin-layer electrode. The sizes of points represent the average experimental deviation. Experimental conditions: as in Figure 14, except as noted. Reprinted with permission from ref 51. Copyright 1982 American Chemical Society.

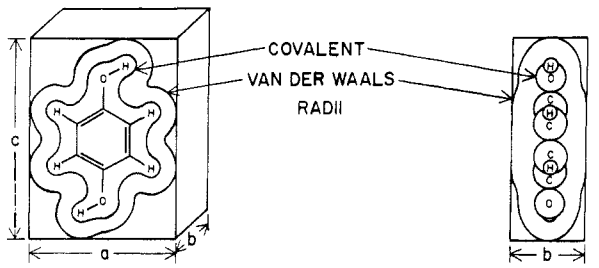

Figure 16. Molecular unit cell assumed in theoretical estimates of packing density. Reprinted with permission from ref 50. Copyright 1982 American Chemical Society.

lecular orientations calculated from van der Waals radii according to the approach introduced by Pauling[52] (Figure 16). Compound **20** (Figure 15A) illustrates the behavior of a large family of compounds characterized by a large, constant packing density resulting from attachment to the surface in a vertical orientation through a single, predominant functional group:

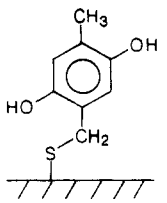

(17)

The methylhydroquinone pendant in eq 17 is reversibly electroactive, as discussed below. Compound **1** (Figure 15F) is representative of another large class of compounds for which two adsorption plateaus are observed as a result of adsorption of the aromatic ring in horizontal or vertical orientations at low or high adsorbate concentrations, respectively:

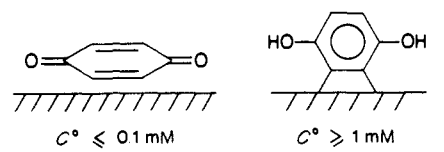

(18)

$C^\circ \leq 0.1$ mM $C^\circ \geq 1$ mM

Compound **22** (Figure 15A) illustrates the behavior of adsorbates having multiple stable orientations:

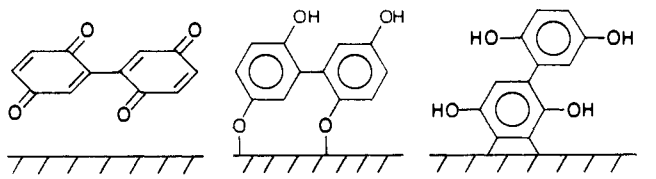

(19)

$C^\circ \leq 0.1$ mM 0.1 mM $\leq C^\circ \leq 1$ mm $C^\circ \geq 1$ mM

The pendant hydroquinone moiety on the right-hand side of eq 19 is reversibly electroactive, as discussed below. Compound **10** (Figure 15G) for which all ring edges are blocked with methyl groups, and compound

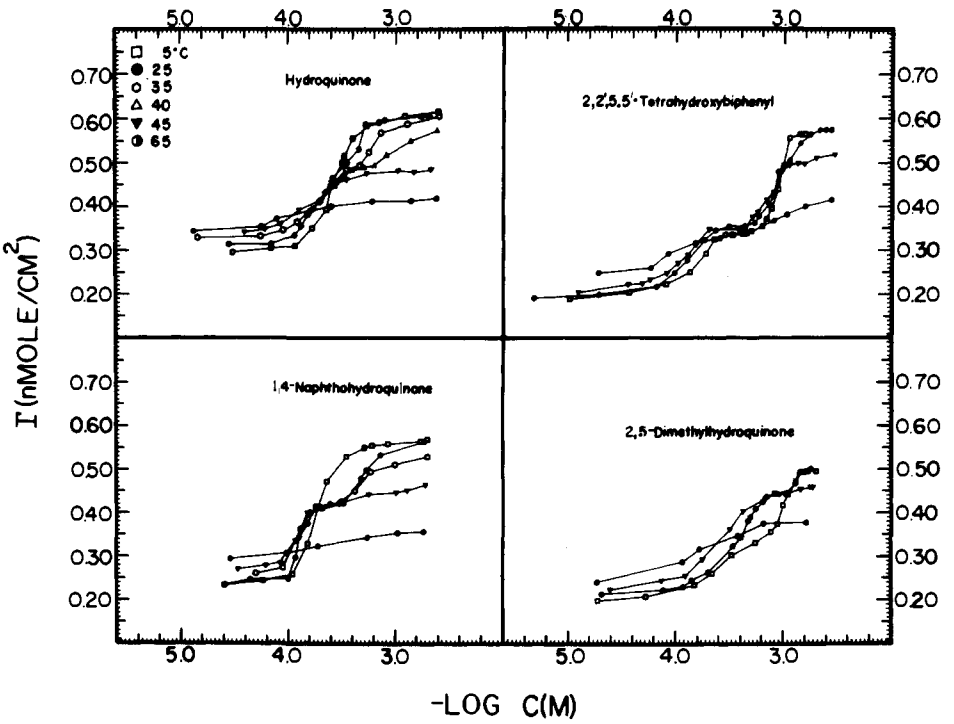

Figure 17. Packing density, Γ (nmol/cm^2), vs adsorbate concentration at various temperatures. Experimental conditions: polycrystalline Pt thin-layer electrode; 1 M $HClO_4$ electrolyte. Reprinted with permission from ref 53. Copyright 1983 American Chemical Society.

25 (Figure 15) containing three fused aromatic rings, adopt only the horizontal orientation. Compound **13** (Figure 15B) adsorbs primarily in a vertical, N-attached orientation when adsorbed from neutral solution (eq 20)

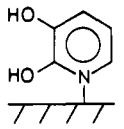

(pH 7) (20)

but adopts horizontal or vertical orientations when adsorbed from strongly acidic solution:

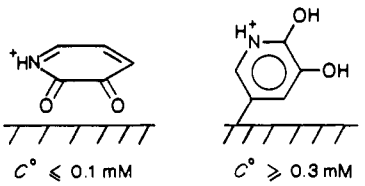

$C^\circ \leq 0.1$ mM $C^\circ \geq 0.3$ mM (21)

Compounds such as **11** (Figure 15L), heavily halogenated at the ring, prefer to bind to the surface in an O-attached vertical orientation:

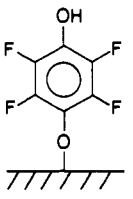

(22)

Although the quantitative details of these molecular adsorption processes vary with surface structure, nature of the electrolyte, and other experimental variables, nevertheless the same basic phenomena have been observed for all systems studied to date. Extensive tabulations of adsorption data for oriented molecular layers are available in ref 50 and 51.

2. Influence of Temperature

The influence of temperature on molecular adsorption at electrodes depends upon the molecular characteristics of the adsorbate with respect to the mode of attachment to the surface. For example, adsorption of thiophenol derivatives to Pt surfaces in a single orientation through the S atom (eq 17) displays a relatively slight temperature dependence, the expected decrease with increasing temperature. On the other hand, hydroquinone derivatives that are capable of multiple adsorbate orientations undergo a transition from oriented adsorption to mixed or disordered orientation[53] as the temperature rises above about 45 °C, as shown in Figure 17.

3. Influence of Electrode Potential

Packing density of hydroquinone at polycrystalline Pt thin-layer electrodes decreases sharply at potentials where adsorbed hydrogen or oxide is present[54] (Figure 18). However, packing density varies only slightly with potential between two extremes. Evidently, the decline of hydroquinone packing density at extreme potentials was due primarily to competition between hydroquinone and adsorbed H or OH, rather than to an intrinsic potential dependence of the hydroquinone adsorption process itself.

4. Influence of Anions

Packing densities of hydroquinone at polycrystalline Pt vs hydroquinone concentration in various 1 M electrolytes (H_3PO_4, H_2SO_4, Cs_2SO_4, $HClO_4$, $NaClO_4$, NaF/HF, or $NaPF_6$) are virtually identical.[55] Evidently, none of these anions adsorbs sufficiently strongly from 1 M solutions to compete noticeably with the adsorption of hydroquinone, a typical aromatic adsorbate, even

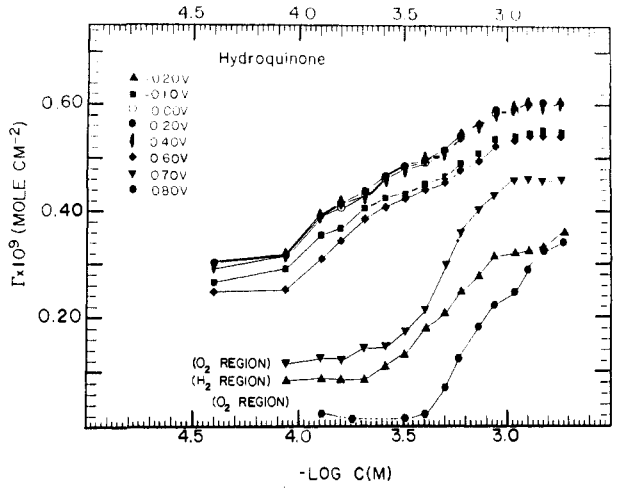

Figure 18. Packing density of hydroquinone vs HQ concentration at polycrystalline Pt electrodes. Experimental conditions: electrode potential, 0.2 V (vs Ag/AgCl) at pH 0 or −0.2 V at pH 7 (F^- only); electrolyte was 1 M $HClO_4$ or 1 M $NaClO_4$ (F^- only); temperature was 23 ± 1 °C. Reprinted with permission from ref 56. Copyright 1984 Elsevier Sequoia.

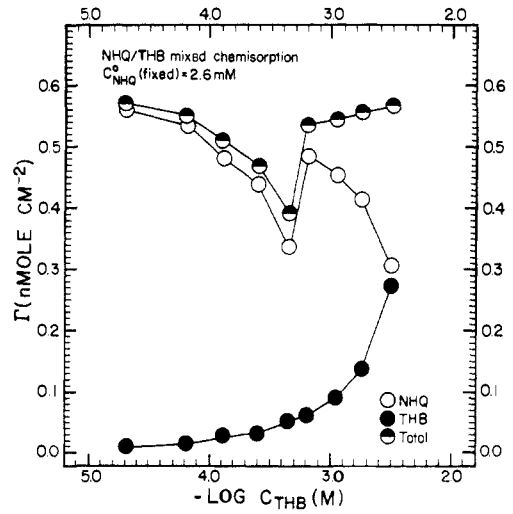

Figure 19. Individual and total packing densities for 1,4-naphthodhydroquinone (NHQ) and 2,5,2′,5′-tetrahydroxybiphenyl (THB) at a polycrystalline Pt electrode. Open circles (○), NHQ. Filled circles (<<ftd), THB. Half-filled circles (◓), total. Experimental conditions: NHQ concentration, 2.5 mM; 1 M $HClO_4$ electrolyte; 23 ± 1 °C. Reprinted with permission from ref 58. Copyright 1986 American Chemical Society.

though hydroquinone is present at comparatively low concentrations (0.03–5 mM). However, Br^- has a profound effect upon aromatic adsorption[56] (Figure 18). Iodide ions prevent aromatic adsorption essentially completely, and displace preadsorbed aromatic hydrocarbons within minutes.[57]

5. Mixtures of Aromatic Adsorbates

Competitive adsorption between aromatic adsorbates can lead to packing densities that are not simply additive.[58,59] This situation is illustrated by competition between 1,4-naphthohydroquinone (NHQ) and 2,5,2′,5′-tetrahydroxybiphenyl (THB) (Figure 19). Adsorption from binary mixtures of these adsorbates at polycrystalline Pt results in various degrees of disordered (inefficient) packing, signalled by the deep

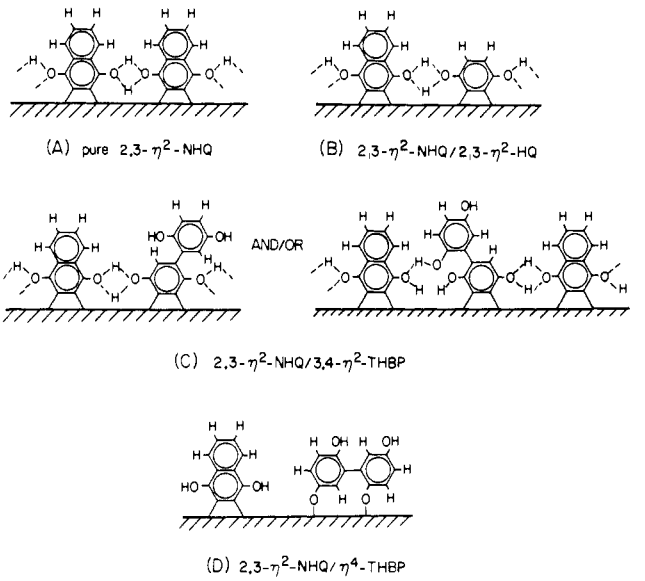

Figure 20. Models illustrating the orientational dependence of intermolecular hydrogen bonding in vertically oriented chemisorbed polyphenols (by analogy with crystalline dephenols[60]). Reprinted with permission from ref 58. Copyright 1986 American Chemical Society.

minimum in the total packing density and NHQ packing density at certain ratios of concentrations. Structural models that account for this effect are shown in Figure 20. According to these models, at certain proportions of THBP in the layer, the THBP molecules are present in an orientation that is not conducive to intermolecular hydrogen bonding. These models are patterned after hydrogen bonding in crystalline diphenols.[60]

6. Influence of Nonaqueous Solvents

Nonaqueous solvents such as benzene,[61] acetonitrile,[62] pyridine, dimethyl sulfoxide,[63] sulfolane, and dimethylacetamide chemisorb strongly at Pt surfaces. Others such as acetic acid, ethyl acetate, and tetrahydrofuran adsorb to a significant extent in competition with aromatic compounds.[64,65] Dilute aqueous solutions of these materials strongly interfere with adsorption of typical aromatic compounds at Pt.[61-63] Accordingly, although data are sparse concerning adsorption of aromatics at Pt surfaces from nonaqueous media under well-defined conditions, chemisorption of the solvent is expected to dominate the chemistry of the electrode surface under those conditions.

7. Influence of Surface Roughness

Adsorption of hydroquinone has been studied at Pt surfaces reproducibly roughened by platinization or mechanical abrasion.[66] Roughnesses (real area/geometric area) from 1.02 to 4.5 were examined (Figure 21). The effect of roughness is to obscure the horizontal-to-vertical packing-density transition, evidently by suppressing formation of the vertical orientation. Beyond a roughness of about 5, the transition essentially vanishes. Substantial differences between packing densities observed at electrochemically cycled polycrystalline surfaces and single-crystal surfaces prepared in UHV are also typical, as described below.

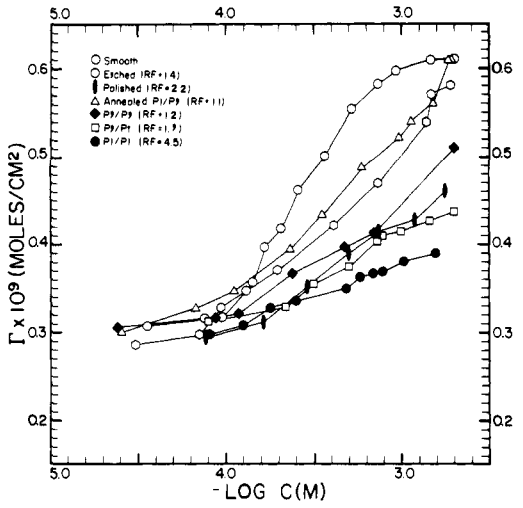

Figure 21. Packing density of hydroquinone vs HQ concentration at polycrystalline Pt thin-layer electrodes roughened by various methods. Experimental conditions: 1 M $HClO_4$; electrode potential, 0.2 V (Ag/AgCl reference); 23 ± 1 °C; RF = (real area)/(geometric area). Reprinted with permission from ref 66. Copyright 1984 Elsevier Sequoia.

8. Reversible Electrochemical Reactions of Adsorbed Molecules

Adsorbed species such as the one shown in eq 17,[51] in which a pendant hydroquinone or other electroactive moiety is attached to the surface through a remote functional group, chain, or ring usually display electrochemical reactivity analogous to that of the parent molecule:

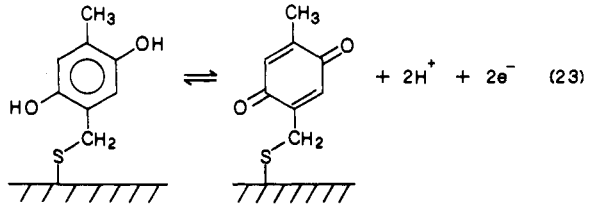

(23)

That is, if the parent molecule undergoes electrochemical oxidation–reduction with only a slight activation barrier, then the adsorbed pendant electroactive moiety will generally do so.[51] On the other hand, adsorbed states in which the hydroquinone or related entity is directly adsorbed to the surface generally do not display

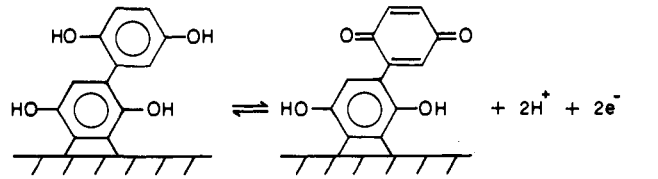

(24)

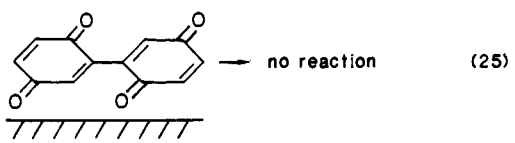

(25)

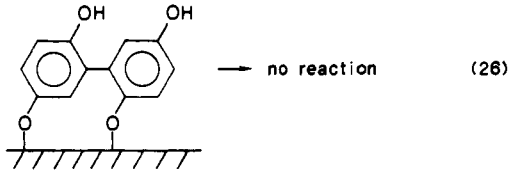

(26)

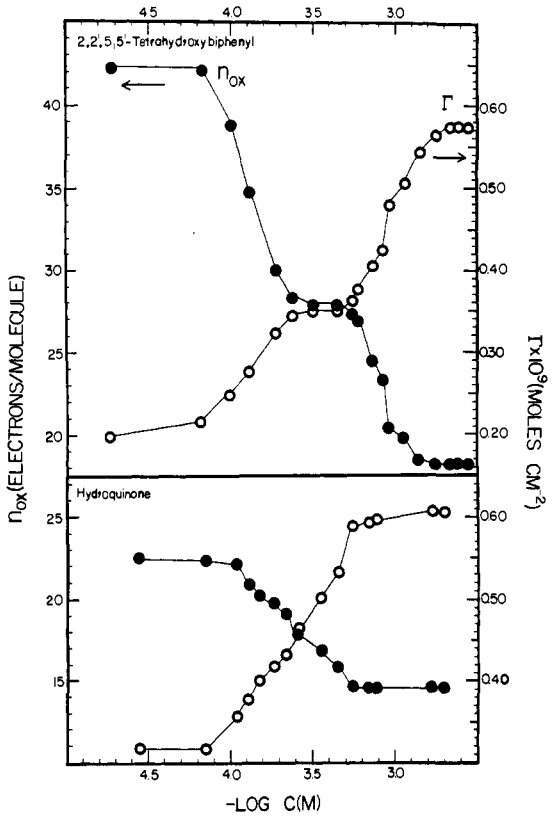

Figure 22. Number of electrons for oxidation of an adsorbed molecule at 2,2',5,5'-tetrahydroxybiphenyl (THBP) or hydroquinone (HQ) (dots, <<ftd). Packing density (nmol/cm²) (open circles, O). Experimental conditions: polycrystalline Pt thin-layer electrode in 1 M $HClO_4$ electrolyte at 23 ± 1 °C. Reprinted with permission from ref 50. Copyright 1982 American Chemical Society.

the reversible redox reactivity of the unadsorbed compounds[50] (Figure 14). Evidently, chemisorption of the electroactive center to a surface causes loss of electroactivity whereas remote attachment to the surface through some other part of the molecule preserves the electroactivity. In keeping with this observation, compounds such as 2,2',5,5'-tetrahydroxybiphenyl (THBP) for which the adsorbed state depends upon the conditions of adsorption, as illustrated in eq 19, display reversible electroactivity under conditions that lead to an adsorbed pendant but not otherwise:[51,58,59,62,63,66] That is, the chemisorption process alters the electronic structure of a directly chemisorbed electroactive center to a sufficient extent that facile redox reactivity disappears.

9. Irreversible Electrochemical Oxidation of Adsorbed Molecules

The products formed by electrochemical oxidation of adsorbed molecules depend upon which parts of the molecule are directly chemically bonded to the surface.[54,66,68-71] This principle is most easily demonstrated by experiments in which a surface containing an adsorbed layer is rinsed with pure supporting electrolyte and oxidized electrochemically at electrode potentials shown to produce complete removal of the layer. Integration of the oxidative current, to obtain the coulometric change, Q_{ox}, and compensation for the background charge observed in the absence of an adsorbed

layer, Q_b, permit calculation of the number of electrons removed in oxidation of the adsorbed molecule, n_{ox}:

$$n_{ox} = (Q_{ox} - Q_b')(\mathbf{F}A\Gamma) \quad (27)$$

where Γ (mol/cm^2) is the packing density of adsorbed molecules in the layer independently determined as indicated by eq 12–16. Results of such experiments are typified by Figure 22; similar results for numerous other compounds are given in ref 69–71. There is an exact correspondence between extent of oxidation (n_{ox}), packing density (Γ), and molecular orientation/mode of attachment to the surface. Horizontal orientation of aromatic adsorbates leads to n_{ox} values amounting to virtually complete oxidation to CO_2 in contrast to vertical (edgewise) attachment for which n_{ox} suggests formation of maleic acid:

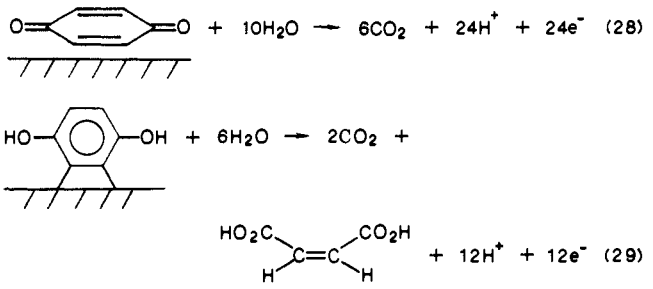

THBP reacts analogously, as do all other compounds studied to date. Products suggested by the n_{ox} value for the various adsorbed states of THBP are

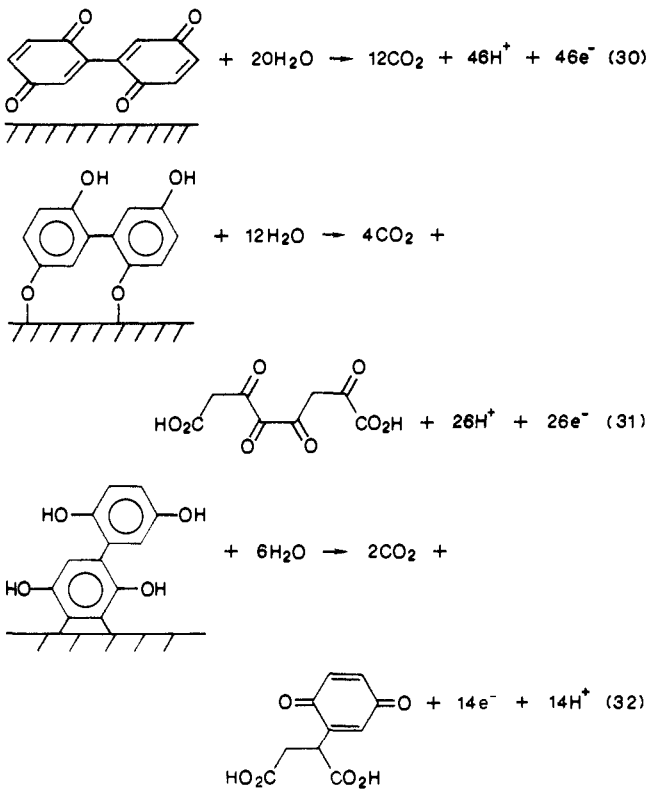

That is, there is every reason to expect that specific well-defined intermediates can be employed as sources of specific electrochemical products. Also, there is every reason to expect similar specificity in the *chemical* reaction pathways of well-defined adsorbed intermediates reacting with solutions. This is a promising area of future investigation.

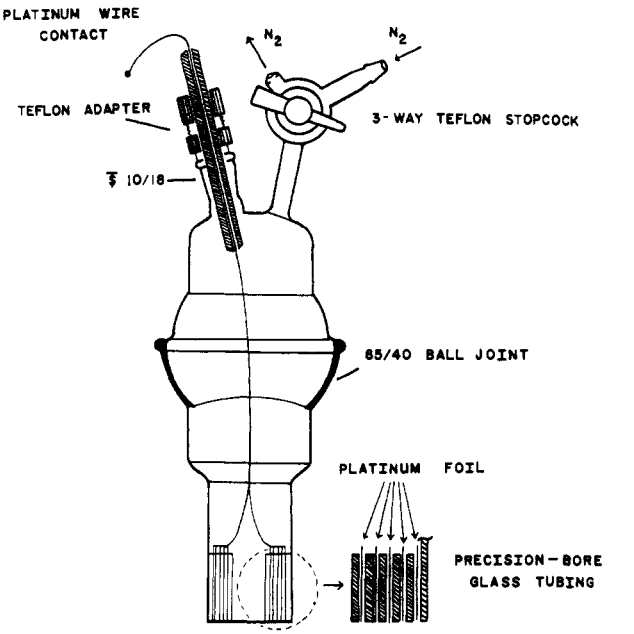

Figure 23. Large-area thin-layer electrode. Area = 168 cm^2; volume = 0.90 cm^3. Reprinted with permission from ref 73. Copyright 1986 American Chemical Society.

10. Irreversible Electrochemical Reduction of Adsorbed Molecules

Electrochemical reduction of chemisorbed mercaptans and thiophenols leads to scission of the carbon–sulfur bond, yielding dissolved hydrocarbons and adsorbed hydrogen sulfide as products:[72–74]

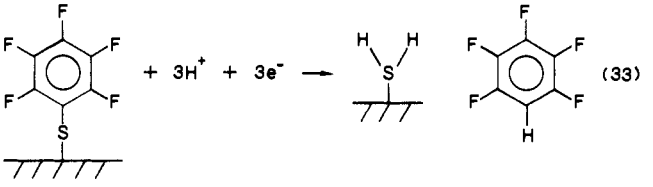

At least when carried out at annealed polycrystalline Pt electrodes, the reduction process is specific to the carbon–sulfur bond; hydrogenation of other parts of the adsorbed molecules does not occur to a detectable extent.

Products from hydrodesulfurization of pentafluorothiophenol, 2,5-dihydroxythiophenol, and 2-mercaptobenzoic acid have been recovered and analyzed directly through the use of large-area thin-layer electrodes in conjunction with capillary gas chromatography.[73] A high-area, large-volume thin-layer electrochemical cell was constructed in order to prepare samples of sufficient size for convenient recovery and analysis (Figure 23). The electrolyte containing the reduction product was collected in liquid nitrogen, followed by solvent extraction with diethyl ether. Purification of the reagents is the most important special consideration in such experiments because traces of organic impurities would otherwise interfere with the relatively small quantities of reduction products (about 3×10^{-8} mol). For example, methyl ether was freshly distilled from ferrous sulfate to remove otherwise destructive peroxides. Inorganic reagents such as $CaCl_2$ drying agent were heated to about 450 °C under N_2 to remove or-

ganic impurities. Low-boiling samples for gas chromatographic analysis were introduced onto the column from a carefully dried ether solution; high-boiling samples were esterified prior to analysis. Liquid chromatographic analyses were carried out isocratically on a reverse-phase polymer column with a water–methanol mobile phase. External standards consisting of similar compounds were introduced into all samples. Gas and liquid chromatographic methods served equally well for the aromatic samples studied to date. Therefore, it is now possible to recover and analyze products from electrolysis of single molecular layers for use in mechanistic studies of electrode surface reactions.

B. Adsorption at Well-Defined Pt(111) Surfaces

Studies of molecular adsorption at well-defined electrode surfaces are of interest in view of the demonstrated sensitivity of adsorption and adsorbate electrochemical reactivity to surface structure.[66,75] Also, surface-sensitive spectroscopy contributes information regarding surface molecular structure and chemical bonding that would not be available from electrochemical experiments alone. For instance, high-resolution electron energy-loss spectroscopy (EELS) yields complete vibrational spectra: the full range of frequencies is covered, from the far-IR range (50–600 cm^{-1}) where substrate–adsorbate vibrations are found, through the mid-IR region (600–4000 cm^{-1}) where the various bending and stretching modes occur, and out into the visible and UV energy of electronic processes; sensitivity of EELS to adsorbed molecules is ample to observe all of the bands that would normally be present in the vibrational spectra of the unadsorbed compounds. Obviously, the availability of such vibrational spectra for well-characterized surfaces and adsorbed layers will provide many useful insights into the nature of the surface layer, including its molecular constitution, mode of chemical bonding between adsorbate and substrate, interactions between neighboring adsorbed species, and the changes in the surface layer that occur as a result of chemical and electrochemical processes. Surface IR and Raman spectroscopy and related techniques will likewise provide useful information when adapted to well-defined surfaces. Auger spectroscopy is a convenient source of sensitive, quantitative data concerning the elemental composition of the surface layer, such as the molecular packing density, molecular stoichiometry, adsorbed solvent, electrolyte surface oxide/hydroxide, and trace elements. Auger spectroscopy also provides clues as to the relative positions of atoms in the surface layer; that is, when Auger spectroscopy is included in the experimental plan, it is possible to know whether the electrode surface is clean at the start of the experiment, and to determine the composition of the adsorbed layer, whether it consists of intentional adsorbates or unintended impurities at each subsequent stage of the experiment. Electrochemical experiments contribute information and insights concerning the interface that are not available from gas–solid experiments alone. Solid–liquid surface chemistry is of interest in its own right and offers the advantages of pH control, potential control, and the moderating influence of a solvent.

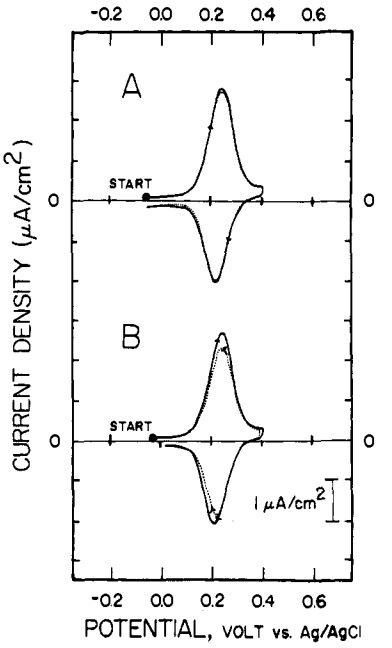

Figure 24. Cyclic voltammograms of 2,5-dihydroxy-4-methylbenzyl mercaptan (DMBM) adsorbed at Pt(111). (A) Solid curve (–), after immersion into 0.7 mM DMBM and rinsing with pure electrolyte. Dotted curve (···), as above, and then 1 h in vacuum prior to voltammetry. (B) Solid curve (–), first scan. Dotted curve (···), second scan. Reprinted with permission from ref 45. Copyright 1988 American Chemical Society.

1. Thiophenol and Related Compounds

Adsorption of a series of compounds related to thiophenol at well-defined Pt(111) surfaces has been studied by means of electrochemical methods (voltammetry) assisted by Auger spectroscopy, EELS, and LEED:[45] thiophenol (TP), pentafluorothiophenol (PFTP), 2,3,5,6-tetrafluorothiophenol (TFTP4), 2,3,4,5-tetrafluorothiophenol (TFTP2), 2,5-dihydroxythiophenol (DHTP), 2,5-dihydroxy-4-methylbenzyl mercaptan (DMBM), and benzyl mercaptan (BM). Two of these

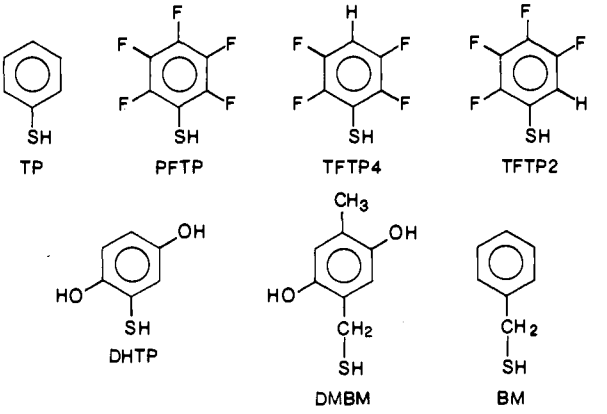

compounds, DMBM and DHTP, undergo reversible oxidation–reduction in the adsorbed state. Shown in Figure 24A (solid curve) is the cyclic voltammogram of a Pt(111) surface that had been immersed into 0.7 mM DMBM in 10 mM trifluoroacetic acid supporting electrolyte at 0.2 V (vs an Ag/AgCl reference electrode) and then rinsed in pure electrolyte. Adsorbed DMBM reacts as indicated in eq 23. Also shown in Figure 24A (dashed curve) is the cyclic voltammogram after DMBM is adsorbed and the electrode is rinsed with

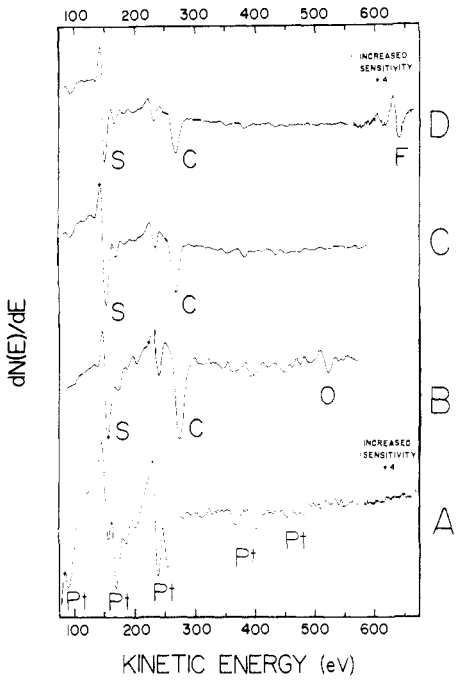

Figure 25. Auger spectra of adsorbed thiophenol and related compounds at Pt(111). (A) Clean Pt(111), (B) 2,5-dihydroxy-4-methylbenzyl mercaptan (DMBM), (C) thiophenol (TP), (D) pentafluorothiophenol (PFTP). Experimental conditions: adsorbate concentrations, 0.7 mM; incident beam 100 nA, 2000 eV, at normal incidence. Reprinted with permission from ref 45. Copyright 1988 American Chemical Society.

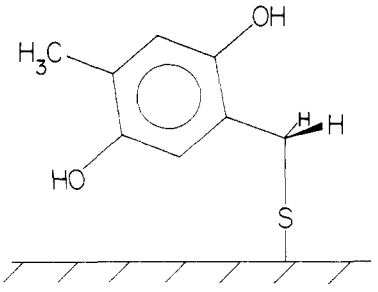

Figure 26. Structural model of DMBM adsorbed at Pt(111) at saturation coverage. Reprinted with permission from ref 45. Copyright 1988 American Chemical Society.

electrolyte solution and allowed to be in vacuum for 1 h. As can be seen, the two voltammograms are virtually identical, demonstrating that the adsorbed layer is completely stable in vacuum. Results are quantitatively consistent with those obtained with thin-layer electrodes, entirely in solution, with or without rinsing. Furthermore, proper use of LEED, Auger spectroscopy, EELS, and related techniques causes no detectable changes. In other words, the DMBM layer has ample stability to be fully characterized by surface spectroscopies in UHV. In contrast, cyclic voltammetry causes appreciable damage to the layer, primarily scission of the carbon–sulfur bond,[73] as can be seen from a comparison of the first and second voltammetric cycles (Figure 24B). Similar behavior has been found for all of the chemisorbed species studied to date.

Auger spectra of thiophenol and related compounds are shown in Figure 25. Packing densities of individual elements of the adsorbed layer, Γ_X (mol/cm^2), were determined from the Auger signals of each element, I_X, by means of eq 34, where $1/L_i$ is the fraction of atoms

$$I_X/I_{Pt}^\circ = B_X\Gamma_X(f_1/L_1 + f_2/L_2 + ... + f_N/L_N) \quad (34)$$

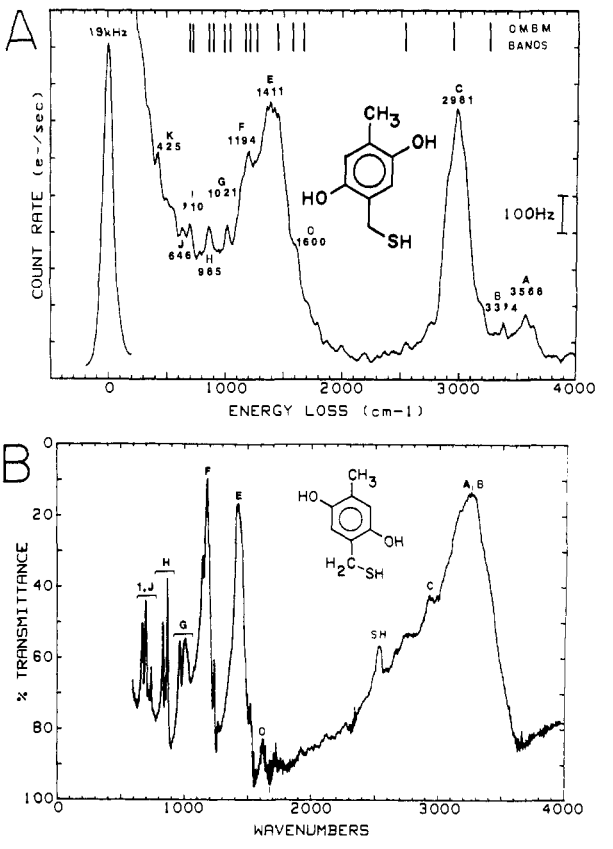

Figure 27. Vibrational spectra of DMBM. (A) EELS spectrum of adsorbed DMBM at Pt(111), (B) IR spectrum of solid DMBM in KBr. Experimental conditions: DMBM solution concentration, 0.1 mM in 10 mM KF/HF electrolyte (pH 4); EELS incidence and detection angles, 62° from surface normal; beam energy, 4 eV; beam current, 15 nA; EELS resolution, 10 meV (80 cm^{-1}) FWHM; IR resolution, 4 cm^{-1} FWHM. Reprinted with permission from ref 45. Copyright 1988 American Chemical Society.

of element X located in layer i (i = 1 is adjacent to the solid and N is the outermost layer) and f_i is the scattering factor at the Auger electron kinetic energy of element X in layer i. Molecular packing densities have been determined independently from the positive lobe of the Pt Auger signal at 235 eV, by means of eq 35,

$$I_{Pt}/I_{Pt}^\circ = (1 - J_1K\Gamma)(1 - J_2K\Gamma)...(1 - J_NK\Gamma) \quad (35)$$

where J_i represents the number of non-hydrogen/fluorine atoms per molecule located at each level of the adsorbed layer, $J_1 + J_2 + ... + J_N = N$, and N is the total number of such atoms per molecule. For example, the packing densities of C, O, and S in DMBM are given by

$$\Gamma_C = (I_C/I_{Pt}^\circ)/[B_C(5f/8 + 3/8)] \quad (36)$$

where I_{Pt} is measured at the positive lobe of the Pt signal at 235 eV to minimize overlap with other peaks in the spectrum, $B_C = 8.48 \times 10^8$ cm^2/mol, and $f = 0.702$ (from the Pt(111)(3×3)–benzoquinone reference structure[44]) and by

$$\Gamma_O = (I_O/I_{Pt}^\circ)/[B_O(f^3/2 + 1/2)] \quad (37)$$

$$\Gamma_S = (I_S/I_{Pt}^\circ)/(B_Sf_S)$$

where $B_O = 6.53 \times 10^8$ cm^2/mol, $B_S = 3.20 \times 10^{10}$ cm^2/mol, $f_O = 0.70$, and $f_S = 0.62$. Molecular packing density, Γ, of DMBM can also be determined independently from attenuation of the Pt signal at 235 eV

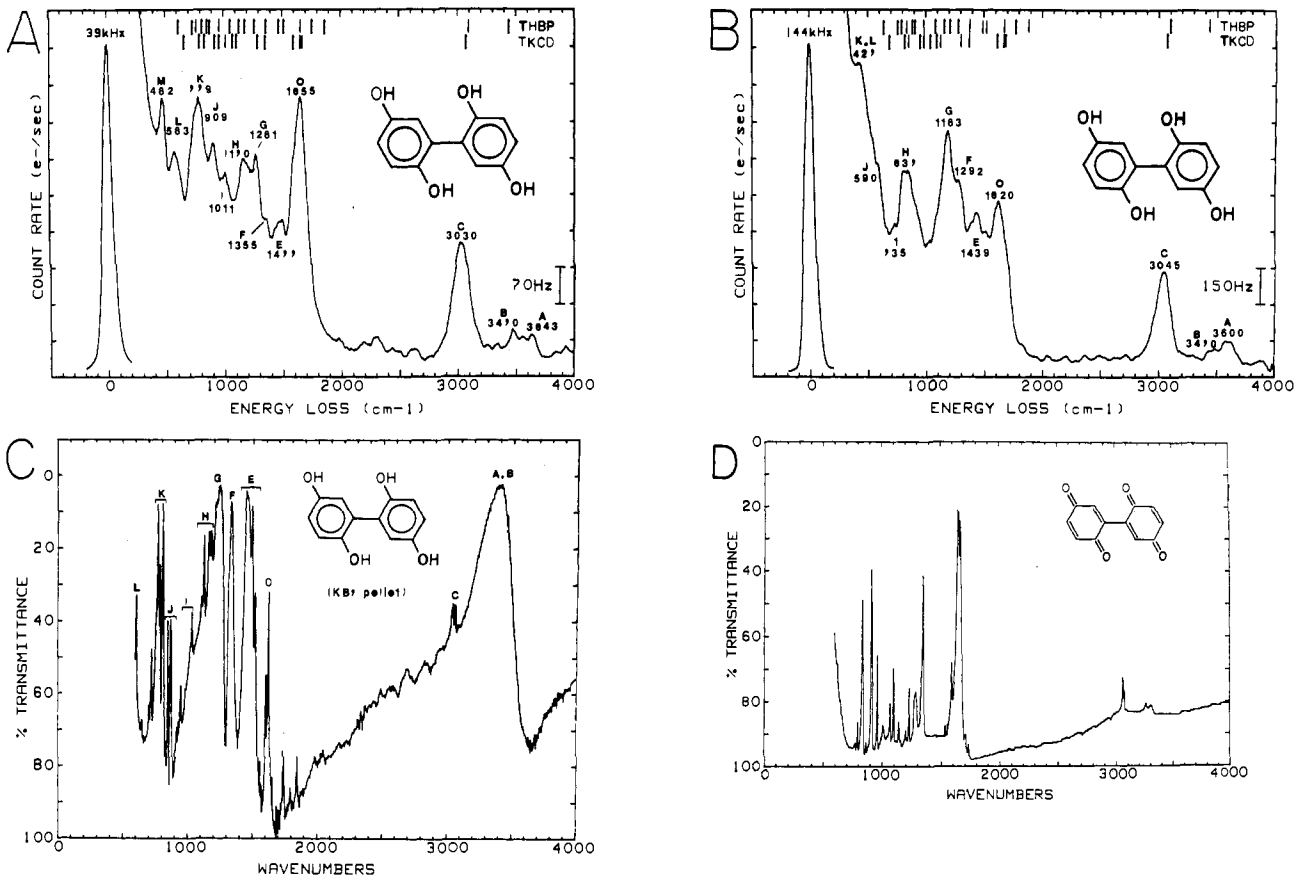

Figure 28. Vibrational spectra of THBP and TKCD. (A) EELS spectrum of Pt(111) after immersion into 0.1 mM THBP, (B) EELS spectrum of Pt(111) after immersion into 5 mM THBP, (C) IR spectrum of solid THBP in KBr, (D) IR spectrum of solid TKCD in KBr. Experimental conditions: as in Figure 27. Reprinted with permission from ref 46. Copyright 1988 Elsevier Sequoia.

due to the adsorbed layer[76] by means of eq 38, where

$$I/I_{Pt}^{\circ} = (1 - K\Gamma)(1 - 5K\Gamma) \qquad (38)$$

$K = 1.53 \times 10^8$ cm^2/mol (see ref 44). The results are as follows: $\Gamma_C = 3.07$ nmol/cm^2, $\Gamma_O = 0.633$ nmol/cm^2, $\Gamma_S = 0.39$ nmol/cm^2, (molecular packing density from $\Gamma_C/11$) = 0.384 nmol/cm^2 and (from Pt Auger signal attenuation) = 0.397 nmol/cm. The ideal molecular packing density in the model structure shown in Figure 26 is $\Gamma = 0.39$ nmol/cm^2.

The EELS spectrum of adsorbed DMBM is shown in Figure 27. Also shown is the infrared spectrum of solid DMBM in KBr (only the mid-IR is shown, 600–4000 cm^{-1}). Although a slight difference in appearance of the spectra results from instrumental resolution (80 cm^{-1} in EELS, 4 cm^{-1} in IR), the high degree of correspondence between the EELS spectrum of adsorbed DMBM and the IR spectrum of solid DMBM is characteristic of all the mercaptans and thiophenols studied. Proposed assignments of the EELS bands are discussed in ref 45. The absence of the SH stretch (2500 cm^{-1}) from the EELS spectra of DMBM and all of the related adsorbates is evidence for loss of the mercaptyl hydrogen during adsorption:

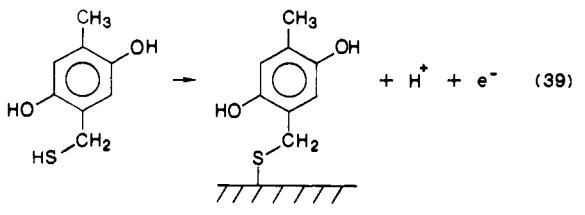

(39)

A Pt(111)(2√3×2√3)R30°–DMBM LEED pattern can be observed at low coverage ($\theta = {}^1/_{12}$ DMBM molecules per surface Pt atom), but the LEED pattern is diffuse at higher packing densities; the limiting packing density is $\theta = 0.155$.

2. Hydroquinone and Related Compounds

Adsorption and electrochemical oxidation at Pt(111) of a series of compounds related to hydroquinone (HQ) have been studied:[44,46] benzoquinone (BQ), phenol (PL), perdeuteriophenol (PDPL), tetrafluorohydroquinone (TFHQ), 2,2′,5,5′-tetrahydroxybiphenyl (THBP), and 2,2′,5,5′-tetraketodicyclohexadiene (TKCD). Two of

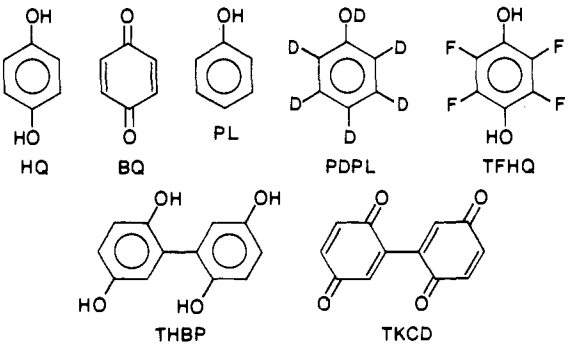

these compounds, THBP and TKCD, display reversible electroactivity in the edge-pendant adsorbed state (eq 24). The electroactive species are stable in vacuum,[46] although cyclic voltammetry causes removal of the surface layer due to catalytic hydrogenation and oxidation, depending upon the electrode potential.

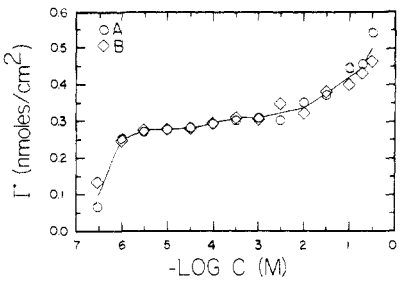

Figure 29. Packing density, Γ, of HQ/BQ at Pt(111). (A) Γ, based upon $I_c/I_{Pt}°$, eq 34; (B) Γ, based upon $I_{Pt}/I_{Pt}°$, eq 35. Experimental conditions: supporting electrolyte, 10 mM KF adjusted to pH 4 with HF; electrode potential, 0.2 V vs Ag/AgCl (1 M KCl) reference; temperature, 23 ± 1 °C. Reprinted with permission from ref 44. Copyright 1988 American Chemical Society.

Packing densities of THBP measured by Auger spectroscopy according to the two methods described above (eq 34 and 35), electroactive packing densities measured by means of voltammetry, and n_{ox} values (eq 27) indicate that the edgewise adsorbed state of THBP (eq 19) is less stable at Pt(111) than at polycrystalline surfaces and that with increasing THBP concentration the horizontal orientation yields to the edge-pendent orientation. EELS spectra of THBP adsorbed at Pt-(111) are shown in Figure 28A,B. Also shown are the mid-IR spectra (600–4000 cm^{-1}) of solid THBP in KBr and of the quinone form (TKCD) in KBr (Figure 28C,D). The EELS spectra contain all of the bands expected for THBP and TKCD. Assignment of the EELS bands is discussed in ref 46. The heights of the EELS O–H stretch peaks, A and B, and the phenolic C–O stretch, peak G, increase with increasing THBP concentration. Evidently, when adsorption occurs at concentrations below 0.1 mM, the phenolic hydrogens are lost during the adsorption process; on the other hand, at higher concentrations an increasing proportion of the phenolic hydrogens are present in the edge-pendant adsorbed state and are thereby retained.

Packing densities of hydroquinone (HQ) and benzoquinone (BQ) measured by means of C and O Auger signals and from attenuation of Pt Auger electrons as described above reveal that HQ and BQ also display an orientational transition with adsorbate concentration[44] (Figure 29). At concentrations below 0.1 mM, the adsorbed molecules are horizontally oriented with the ring parallel to the surface, whereas above 0.1 mM they adopt an edgewise vertical orientation. A similar transition is observed at polycrystalline thin-layer electrodes;[51] the Pt(111) surface favors the horizontal orientation relative to the edgewise orientation. Measurements of n_{ox} by means of coulometry ($Q_{ox} - Q_b'$) combined with Auger spectroscopy (Γ) confirm the orientational transitions inferred from TLE experiments.[51] EELS spectra of the adsorbed layers formed in HQ and BQ solutions are very similar, indicating that a mixture of quinone and phenoxide adsorbed states is formed in either case (Figure 30). Also shown in Figure 30 are the locations of the principal IR bands of solid HQ, BQ, and quinhydrone (SQ). Virtual absence of the O–H stretching band (3260 cm^{-1}) from the EELS spectra of adsorbed layers formed at HQ concentrations below 1 mM indicates that the phenolic hydrogens are lost during adsorption:

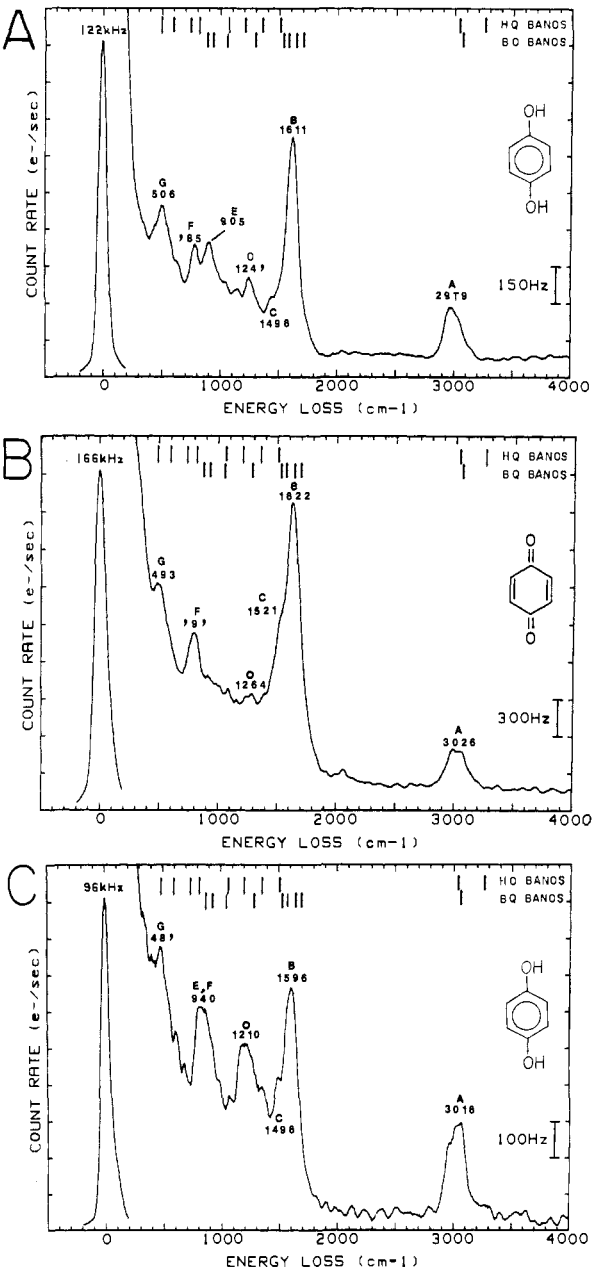

Figure 30. EELS spectra of adsorbed HQ/BQ at Pt(111). (A) HQ (1.0 mM), (B) BQ (1.0 mM), (C) HQ (500 mM). Experimental conditions: supporting electrolyte, 10 mM KF adjusted to pH 4 with HF; electrode potential, 0.2 V vs Ag/AgCl (1 M KCl) reference; temperature, 23 ± 1 °C; beam energy, 4 eV; beam current, 0.15 nA; reflected beam was detected at the specular angle (62° from the surface normal). Reprinted with permission from ref 44. Copyright 1988 American Chemical Society.

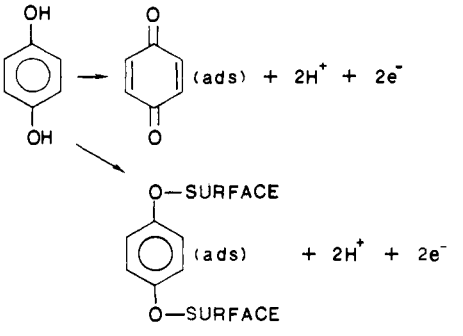

(40)

Variations of the n_{ox} with HQ concentration and packing density as observed by Auger spectroscopy and coulometry at Pt(111) conform closely to eq 28 and 29.

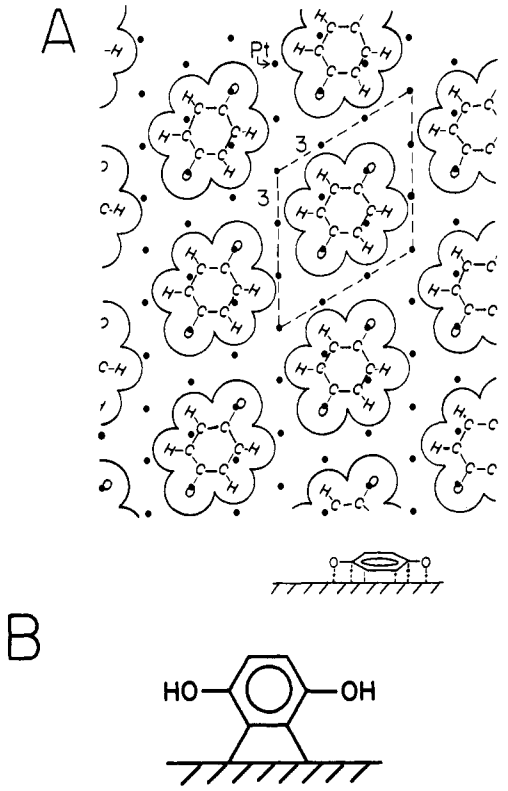

Figure 31. Structure of BQ/HQ adsorbed at Pt(111). (A) Pt(111)(3×3)-BQ/HQ, $\theta = {}^1/_9$ ($\Gamma = 0.276$ nmol/cm^2); (B) Vertical orientation of adsorbed HQ (2,3-η^2). Reprinted with permission from ref 44. Copyright 1988 American Chemical Society.

LEED patterns observed at HQ/BQ packing densities slightly lower than the plateau value have been attributed to Pt(111)(3×3)-BQ. On the basis of the observed symmetry, packing density, and EELS spectrum, the structure shown in Figure 31 has been proposed. Phenol (PL) displays a similar (3×3) pattern under these same conditions.[44]

In order to verify that the HQ/BQ layer is not removed from the Pt(111) surface by evacuation, n_{ox} measurements (eq 27) were made by use of a variation of the usual procedure in which the coated surface is placed in UHV for about 1 h prior to measurement of Q_{ox} and Q_b. The resulting Q_{ox} values do not differ from those obtained without evacuation, indicating stability of the adsorbed layer in vacuum; n_{ox} is also unaffected by evacuation.[44]

Further evidence leading to the assignment of EELS bands of adsorbed phenols and quinones is provided by the spectrum for perdeuteriophenol (PDPL, phenol-d_6) (Figure 32B). As expected, the CH stretching band of PL at 3020 cm^{-1} is replaced by a CD band at 2258 cm^{-1} (peak A). Peaks F–I, assigned to CH/CD modes, are shifted, whereas peaks B–E remained fixed, as expected.[44] EELS spectra for PL and PDPL adsorbed from H_2O and D_2O solutions yields further evidence that the phenolic hydrogen is removed during chemisorption of PL.[44] In some of the PDPL experiments it was noticed that traces of contaminating hydrocarbons result in a distinct CH stretching peak in the EELS spectrum near 3000 cm^{-1}. This is because PL is susceptible to competitive adsorption of a wide variety of chemisorbable organic compounds[74] that are present in typical chemical reagents and in the environment. Therefore, the presence/absence of a CH stretching

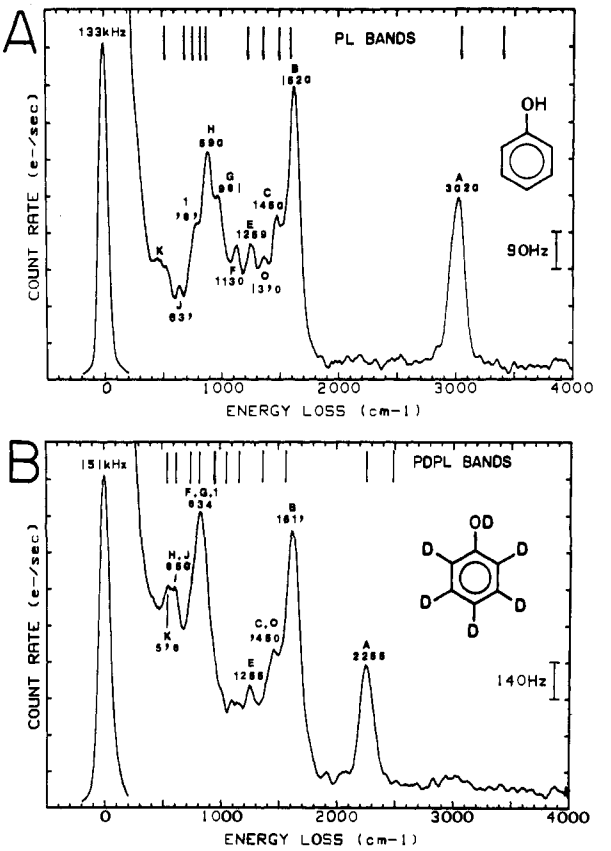

Figure 32. EELS spectra of adsorbed PL and PDPL at Pt(111). (A) Phenol (PL), (B) perdeuteriophenol (PDPL, phenol-d_6). Experimental conditions: adsorbate concentration, 10 mM; other conditions were as in Figure 30. Reprinted with permission from ref 44. Copyright 1988 American Chemical Society.

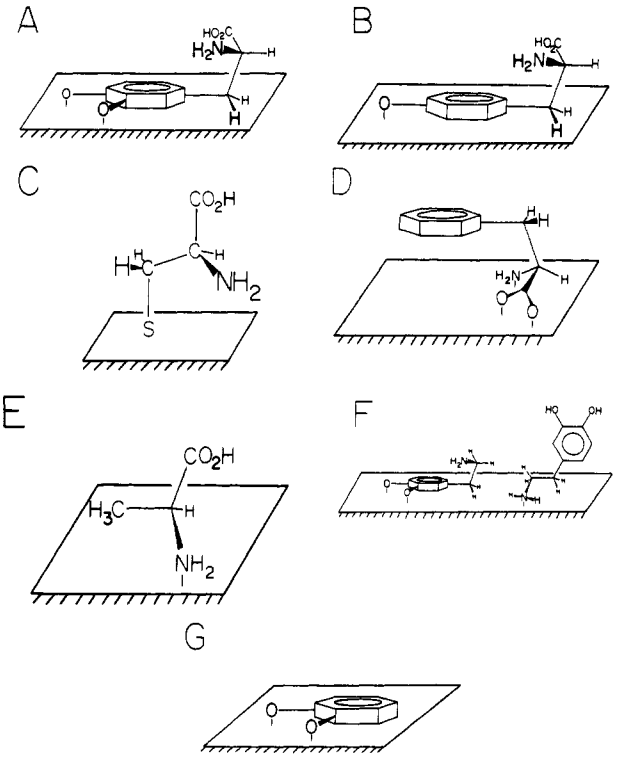

Figure 33. Structural models of adsorbed molecules at Pt(100) and Pt(111) surfaces. (A) L-Dopa, (B) L-tyrosine, (C) L-cysteine, (D) L-phenylalanine, (E) L-alanine, (F) dopamine, (G) catechol. Reprinted with permission from ref 47. Copyright 1988 American Chemical Society.

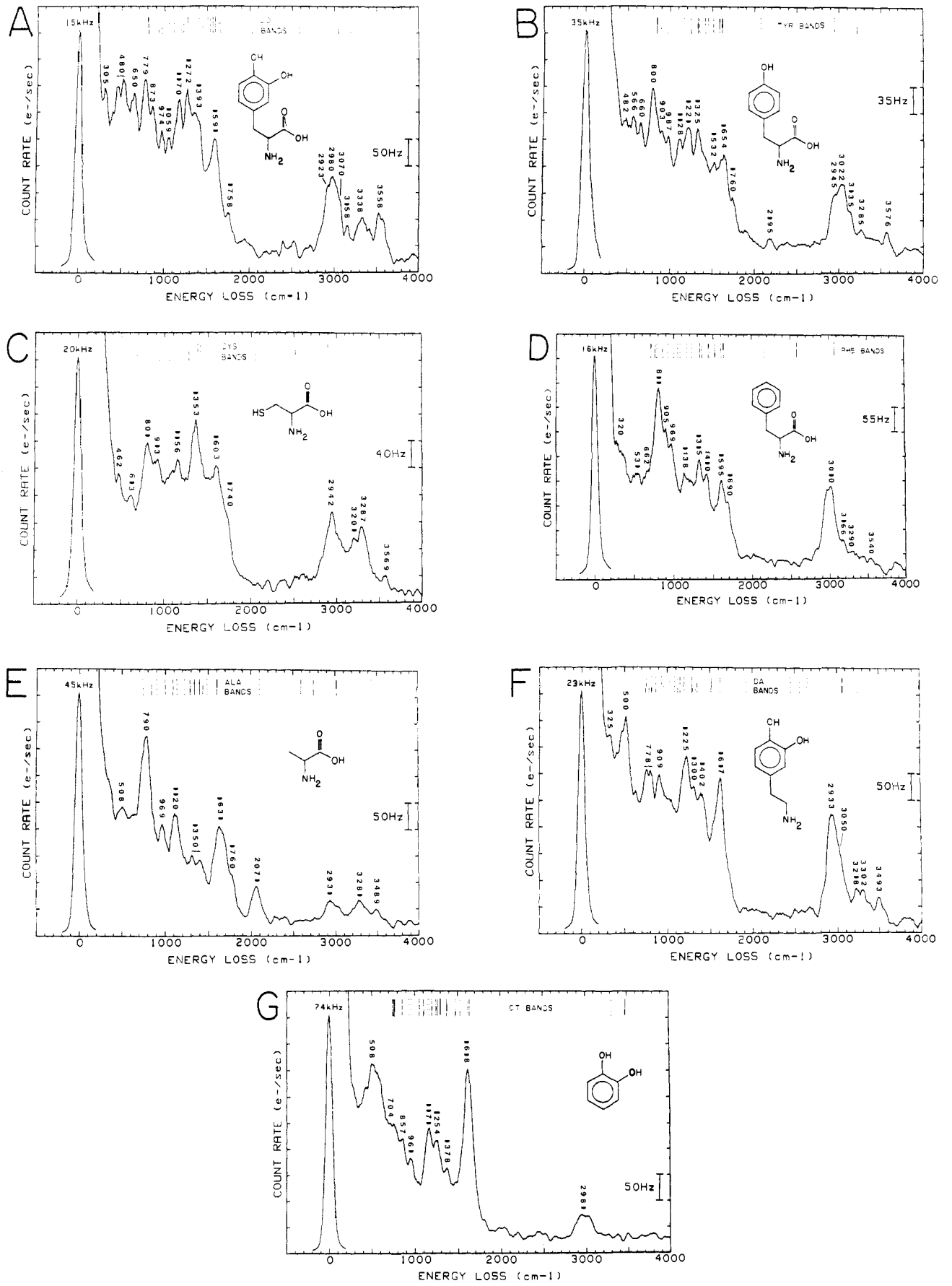

Figure 34. EELS spectra of adsorbed amino acids and related compounds at Pt(111). (A) L-Dopa, (B) L-tyrosine, (C) L-cysteine, (D) L-phenylalamine, (E) L-alanine, (F) dopamine, (G) catechol. Experimental conditions: adsorbate concentrations (mM) were LD (5.0), Tyr (1.0), Cys (0.5), Phe (1.0), Ala (1.0), DA (1.0), CT (1.0); other conditions were as in Figure 30. Reprinted with permission from ref 47. Copyright 1988 American Chemical Society.

peak in the EELS spectrum of adsorbed PDPL is persuasive evidence as to whether the reagents and apparatus are sufficiently clean to yield the intended adsorbed layer. *Therefore, it is recommended that others attempting to obtain EELS, IR, or related data for organic species adsorbed at electrode surfaces record spectra of adsorbed PDPL as a procedural test before publishing spectra of other adsorbed compounds.* Tetrafluorohydroquinone can also be employed for this purpose.

3. Amino Acids and Related Compounds

Adsorption at Pt(111) of a group of compounds related to L-dopa has been studied:[47] L-dopa (LD), L-tyrosine (Tyr), L-cysteine (Cys), L-phenylalanine (Phe), L-alanine (Ala), dopamine (DA), and catechol (CT). As

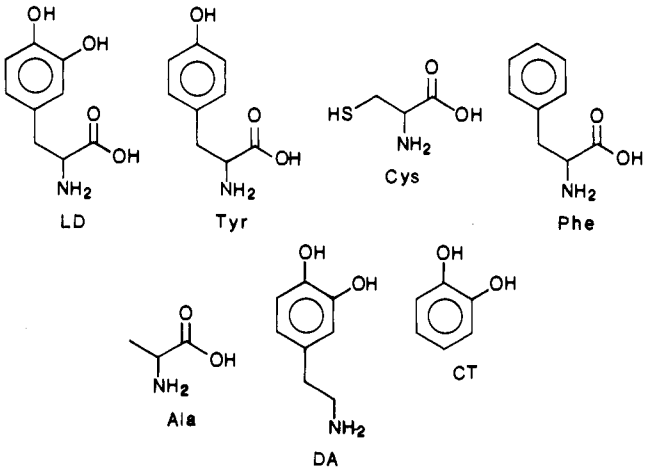

was the case for the mercaptans, phenols, and thiophenols, no detectable changes in the amino acid layer occurs as a result of evacuation, as evidenced by measurements of Q_{ox} (see eq 27) before and after evacuation.

Packing-density measurements for these compounds by means of the two Auger spectroscopic methods described in connection with eq 34 and 35 indicate a single adsorption plateau at Pt(100) and Pt(111). For instance, at Pt(100) the plateau packing density, $\Gamma = 0.18$ nmol/cm^2, is much smaller than for a ring-vertical orientation (0.45 nmol/cm^2) and corresponds instead to a horizontal orientation. Best agreement with experiment is displayed by the model structure shown in Figure 33A, for which the theoretical packing density based upon van der Waals distances[52] is 0.176 nmol/cm^2. In this structure the catechol ring is parallel to the Pt surface, and the alanine moiety is pendant, extending away from the ring. Structures in which the amino acid makes direct contact with the surface predict packing densities which are significantly too low, about 0.166 nmol/cm^2. Structures consistent with packing-density data obtained from Auger spectra for the remaining compounds in this series at Pt(100) and Pt(111) surfaces are shown in Figure 33B–G. LD and Tyr are of course similar because in both cases attachment occurs through the phenolic aromatic ring. Cys attaches to Pt surfaces through the mercaptan sulfur atom, with loss of the sulfyhdryl hydrogen atom. Phe is somewhat surprising in its behavior; in the absence of phenolic OH groups, its attachment to Pt is predominantly through the amino acid moiety, Figure 33D, in analogy with the adsorption of Ala (Figure 33E). DA and CT adsorb primarily by horizontal attachment of the catechol ring to the surface (Figure 33F,G) except at very high concentrations, as for HQ.

EELS spectra of these adsorbed compounds are shown in Figure 34. Also shown are the locations of bands in the IR spectra of the solid compounds in KBr. The EELS spectra do not exhibit bands corresponding to the sulfhydryl hydrogen of Cys (Figure 34C), as explained by the structure shown in Figure 33C. The phenolic OH bands of LD, Tyr, DA, and CT are also absent (Figure 34A,B,F,G) as noted in structures 33A,B,F,G. In contrast, the carboxylic OH stretching bands are present in the EELS spectra of LD, Tyr and Cys (Figure 34A–C,H); evidently, the rate and/or strength of adsorption of the catechol, phenol, and sulfhydryl moieties is sufficient to prevent reaction between the Pt surface and the carboxylic hydrogens of those compounds. Similarly, the amine hydrogens of LD, Tyr, Cys, Phe, and Ala are retained during the adsorption processes, as evidenced by the bands near 3200 and 3400 cm^{-1} in the EELS spectra of those compounds. The aromatic CH stretching band of LD (3070 cm^{-1}) is at a higher frequency than the aliphatic bands (2980 and 2923 cm^{-1}) and is therefore evidence of retention of aromatic character in adsorbed LD, Tyr, and Phe, as postulated in structure 33A,B,D. A carboxylic C=O stretch is observed for adsorbed LD (1758 cm^{-1}), Tyr (1760 cm^{-1}), and Cys (1756 cm^{-1}) and is relatively weak in the spectrum of Phe (1690 cm^{-1}) for which interaction of the amino acid moiety with the Pt surface is comparatively strong (Figure 33D). The striking similarity of EELS spectra of LD, Tyr, and Cys, Figure 34A–C, is consistent with their mutual lack of symmetry (C_1), similar molecular constitution, and pendant amino acid structure.

Acknowledgments. I gratefully acknowledge research support from the Air Force Office of Scientific Research, the Department of Energy, the Gas Research Institute, the National Institutes of Health, the National Science Foundation, and the donors of the Petroleum Research Fund, administered by the American Chemical Society. Donald C. Zapien assisted with preparation of this article.

Registry No. TP, 108-98-5; HQ, 123-31-9; Pt, 7440-06-4; Ag, 7440-22-4; CN^-, 57-12-5; SCN^-, 302-04-5.

VI. References

(1) Germer, L. H.; Davisson, C. *Nature (London)* **1927**, *119*, 558.
(2) (a) Germer, L. H.; Hartman, C. D. *Rev. Sci. Instrum.* **1960**, *31*, 784. (b) Ehrenberg, W. *Philos. Mag.* **1934**, *18*, 878.
(3) (a) Propst, F. M.; Piper, T. C. *J. Vac. Sci. Technol.* **1967**, *4*, 53. (b) Lander, J. J. *Phys. Rev.* **1953**, *91*, 1382.
(4) Somorjai, G. A. *Chemistry in Two Dimensions: Surfaces*; Cornell University: Ithaca, NY, 1981.
(5) Hubbard, A. T. *CRC Crit. Rev. Anal. Chem.* **1973**, *3*, 201.
(6) Hubbard, A. T. *Acc. Chem. Res.* **1980**, *13*, 177.
(7) Hubbard, A. T.; Stickney, J. L.; Soriaga, M. P.; Chia, V. K. F.; Rosasco, S. D.; Schardt, B. C.; Solomun, T.; Song, D.; White, J. H.; Wieckowski, A. *J. Electroanal. Chem. Interfacial Electrochem.* **1984**, *168*, 43.
(8) Conway, B. E.; Angerstein-Kozlowska, H.; Sharp, W. B. A.; Criddle, E. E. *Anal. Chem.* **1973**, *45*, 1331.
(9) Salaita, G. N.; Stern, D. A.; Lu, F.; Baltruschat, H.; Schardt, B. C.; Stickney, J. L.; Soriaga, M. P.; Frank, D. G.; Hubbard, A. T. *Langmuir* **1986**, *2*, 828.
(10) Delahay, P. *Double Layer and Electrode Kinetics*, 2nd ed.; Wiley: New York, 1965; Chapter 7.
(11) Garwood, G. A., Jr.; Hubbard, A. T. *Surf. Sci.* **1982**, *112*, 281.

(12) Baltruschat, H.; Martinez, M.; Lewis, S. K.; Lu, F.; Song, D.; Stern, D. A.; Datta, A.; Hubbard, A. T. *J. Electroanal. Chem. Interfacial Electrochem.* **1987**, *217*, 111.
(13) Lu, F.; Salaita, G. N.; Baltruschat, H.; Hubbard, A. T. *J. Electroanal. Chem. Interfacial Electrochem.* **1987**, *222*, 305.
(14) Garwood, G. A., Jr.; Hubbard, A. T. *Surf. Sci.* **1980**, *92*, 617.
(15) Felter, T. E.; Hubbard, A. T. *J. Electroanal. Chem. Interfacial Electrochem.* **1979**, *100*, 473.
(16) Wieckowski, A.; Schardt, B. C.; Rosasco, S. D.; Stickney, J. L.; Hubbard, A. T. *Surf. Sci.* **1984**, *146*, 115.
(17) Solomun, T.; Wieckowski, A.; Rosasco, S. D.; Hubbard, A. T. *Surf. Sci.* **1984**, *147*, 241.
(18) Stern, D. A.; Baltruschat, H.; Martinez, M.; Stickney, J. L.; Song, D.; Lewis, S. K.; Frank, D. G.; Hubbard, A. T. *J. Electroanal. Chem. Interfacial Electrochem.* **1987**, *217*, 101.
(19) Soriaga, M. P.; Chia, V. K. F.; White, J. H.; Song, D.; Hubbard, A. T. *J. Electroanal. Chem. Interfacial Electrochem.* **1984**, *162*, 143.
(20) Salaita, G. N.; Lu, F.; Laguren-Davidson, L.; Hubbard, A. T. *J. Electroanal. Chem. Interfacial Electrochem.* **1987**, *229*, 1.
(21) Frank, D. G.; Katekaru, J. Y.; Rosasco, S. D.; Salaita, G. N.; Schardt, B. C.; Soriaga, M. P.; Stern, D. A.; Stickney, J. L.; Hubbard, A. T. *Langmuir* **1985**, *1*, 587.
(22) Hubbard, A. T.; Stickney, J. L.; Rosasco, S. D.; Soriaga, M. P.; Song, D. *J. Electroanal. Chem. Interfacial Electrochem.* **1983**, *150*, 165.
(23) Stickney, J. L.; Rosasco, S. D.; Song, D.; Soriaga, M. P.; Hubbard, A. T. *Surf. Sci.* **1983**, *130*, 326.
(24) Wieckowski, A.; Rosasco, S. D.; Schardt, B. C.; Stickney, J. L.; Hubbard, A. T. *Inorg. Chem.* **1984**, *23*, 565.
(25) Samuels, L. E. *Metallographic Polishing by Mechanical Methods*; Pitman: London, 1967.
(26) Stickney, J. L.; Rosasco, D. S.; Sond, D.; Soriaga, M. P.; Hubbard, A. T. *Surf. Sci.* **1983**, *130*, 326.
(27) Stickney, J. L.; Rosasco, S. D.; Hubbard, A. T. *J. Electrochem. Soc.* **1984**, *131*, 260.
(28) Schardt, B. C.; Stickney, J. L.; Stern, D. A.; Wieckowski, A.; Zapien, D. C.; Hubbard, A. T. *Surf. Sci.* **1986**, *175*, 520.
(29) Stickney, J. L.; Rosasco, S. D.; Schardt, B. C.; Hubbard, A. T. *J. Phys. Chem.* **1984**, *88*, 251.
(30) Schardt, B. C.; Stickney, J. L.; Stern, D. A.; Wieckowski, A.; Zapien, D. C.; Hubbard, A. T. *Langmuir* **1987**, *3*, 239.
(31) Stickney, J. L.; Stern, D. A.; Schardt, B. C.; Zapien, D. C.; Wieckowski, A.; Hubbard, A. T. *J. Electroanal. Chem. Interfacial Electrochem.* **1986**, *213*, 293.
(32) Ishikawa, R. M.; Katekaru, J. Y.; Hubbard, A. T. *J. Electroanal. Chem. Interfacial Electrochem.* **1978**, *86*, 271.
(33) (a) Ross, P. N., Jr. *Surf. Sci.* **1981**, *102*, 463; (b) Aberdam, D.; Durand, R.; Faure, R.; Elomar, F. *Surf. Sci.* **1986**, *171*, 303.
(34) Will, F. G. *J. Electrochem. Soc.* **1965**, *112*, 451.
(35) Laguren-Davidson, L.; Lu, F.; Salaita, G. N.; Hubbard, A. T. *Langmuir* **1988**, *4*, 224.
(36) Harrington, D. A.; Wieckowski, A.; Rosasco, S. D.; Salaita, G. N.; Hubbard, A. T.; Lumsden, J. B. *Proceedings of the Pourbaix Symposium*; The Electrochemical Society: Princeton, 1984.
(37) Harrington, D. A.; Wieckowski, A.; Rosasco, S. D.; Schardt, B. C.; Salaita, G. N.; Lumsden, J. B.; Hubbard, A. T. *Corros. Sci.* **1985**, *25*, 849.
(38) Harrington, D. A.; Wieckowski, A.; Rosasco, S. D.; Salaita, G. N.; Hubbard, A. T. *Langmuir* **1985**, *1*, 232.
(39) Frank, D. G.; Schneider, M.; Werner, K.; Hubbard, A. T. *Langmuir* **1987**, *3*, 860.
(40) Allen, S. C.; Wild, R. K. *J. Electron Spectros. Relat. Phenom.* **1974**, *5*, 409.
(41) Ekelund, S.; Leggraf, C. *Surf. Sci.* **1971**, *40*, 179.
(42) Seo, M.; Lumsden, J. B.; Staehle, R. W. *Surf. Sci.* **1971**, *50*, 541.
(43) Mussig, H. J.; Arabczyk, W. *Krist. Tech.* **1980**, *15*, 1091.
(44) Lu, F.; Salaita, G. N.; Laguren-Davidson, L.; Stern, D. A.; Wellner, E.; Frank, D. G.; Batina, N.; Zapien, D. C.; Walton, N.; Hubbard, A. T. *Langmuir*, in press.
(45) Stern, D. A.; Wellner, E.; Salaita, G. N.; Laguren-Davidson, L.; Lu, F.; Batina, N.; Frank, D. G.; Zapien, D. C.; Walton, N.; Hubbard, A. T. *J. Am. Chem. Soc.*, in press.
(46) Salaita, G. N.; Laguren-Davidson, L.; Lu, F.; Wellner, E.; Stern, D. A.; Batina, N.; Frank, D. G.; Benton, C. S.; Hubbard, A. T. *J. Electroanal. Chem. Interfacial Electrochem.*, in press.
(47) Frank, D. G.; Batina, N.; Stern, D. A.; Wellner, E.; Salaita, G. N.; Laguren-Davidson, L.; Lu, F.; A. T. *Langmuir*, in press.
(48) (a) Chesters, W. A.; Parker, S. F.; Raval, R. *Surf. Sci.* **1986**, *165*, 179. (b) Hayden, B. E.; Kretzschmar, K.; Bardshaw, Greenler, R. G. *Surf. Sci.* **1985**, *149*, 394; (c) Schoofs, G. R.; Preston, R. E.; Benziger, J. B. *Langmuir*, **1985**, *1*, 313, and references therein.
(49) Hubbard, A. T. Ph.D. Thesis, California Institute of Technology, 1967 (University Microfilms, Ann Arbor, MI, Document No. 67-6066).
(50) Soriaga, M. P.; Hubbard, A. T. *J. Am. Chem. Soc.* **1982**, *104*, 2735.
(51) Soriaga, M. P.; Hubbard, A. T. *J. Am. Chem. Soc.* **1982**, *104*, 3397.
(52) Pauling, L. C. *Nature of the Chemical Bond*, 3rd. ed.; Cornell University: New York, 1960; pp 221–264.
(53) Soriaga, M. P.; White, J. H.; Hubbard, A. T. *J. Phys. Chem.* **1983**, *87*, 3048.
(54) Chia, V. K. F.; Soriaga, M. P.; Hubbard, A. T. *J. Electroanal. Chem. Interfacial Electrochem.* **1984**, *167*, 97.
(55) Soriaga, M. P.; Chia, V. K. F.; White, J. H.; Song, D.; Hubbard, A. T. *J. Electroanal. Chem. Interfacial Electrochem.* **1984**, *162*, 143.
(56) Soriaga, M. P.; White, J. H.; Song, D.; Hubbard, A. T. *J. Electroanal. Chem. Interfacial Electrochem.* **1984**, *171*, 359.
(57) Soriaga, M. P.; Hubbard, A. T. *J. Am. Chem. Soc.* **1982**, *104*, 2742.
(58) Song, D.; Soriaga, M. P.; Hubbard, A. T. *Langmuir* **1986**, *2*, 20.
(59) Song, D.; Soriaga, M. P.; Hubbard, A. T. *J. Electroanal. Chem.* Interfacial *Electrochem.* **1985**, *193*, 255.
(60) Maartmann-Moe, K. *Acta Crystallogr.* **1966**, *21*, 979.
(61) Song, D.; Soriaga, M. P.; Vieira, K. L.; Zapien, D. C.; Hubbard, A. T. *J. Phys. Chem.* **1985**, *89*, 3999.
(62) Song, D.; Soriaga, M. P.; Hubbard, A. T. *J. Electroanal. Chem. Interfacial Electrochem.* **1986**, *201*, 153.
(63) Song, D.; Soriaga, M. P.; Hubbard, A. T. *J. Electrochem. Soc.* **1987**, *134*, 874.
(64) Garwood, G. A., Jr.; Hubbard, A. T. *Surf. Sci.* **1982**, *118*, 223.
(65) Katekaru, J. Y.; Hershberger, J.; Garwood, G. A., Jr.; Hubbard, A. T. *Surf. Sci.* **1982**, *121*, 396.
(66) White, J. H.; Soriaga, M. P.; Hubbard, A. T. *J. Electroanal. Chem. Interfacial Electrochem.* **1984**, *177*, 89.
(67) Soriaga, M. P.; Wilson, P. H.; Hubbard, A. T.; Benton, C. S. *J. Electroanal. Chem. Interfacial Electrochem.* **1982**, *142*, 317.
(68) Soriaga, M. P.; Stickney, J. L.; Hubbard, A. T. *J. Mol. Catal.* **1983**, *21*, 211.
(69) Soriaga, M. P.; Stickney, J. L.; Hubbard, A. T. *J. Electroanal. Chem. Interfacial Electrochem.* **1983**, *144*, 207.
(70) Chia, V. K. F.; Soriaga, M. P.; Hubbard, A. T.; Anderson, S. E. *J. Phys. Chem.* **1983**, *87*, 232.
(71) Soriaga, M. P.; Hubbard, A. T. *J. Phys. Chem.* **1984**, *88*, 1758.
(72) Soriaga, M. P.; Hubbard, A. T. *J. Electroanal. Chem. Interfacial Electrochem.* **1983**, *159*, 101.
(73) Vieira, K. L.; Zapien, D. C.; Soriaga, M. P.; Hubbard, A. T.; Low, K. P.; Anderson, S. E. *Anal. Chem.* **1986**, *58*, 2964.
(74) Stickney, J. L.; Soriaga, M. P.; Hubbard, A. T.; Anderson, S. E. *J. Electroanal. Chem. Interfacial Electrochem.* **1981**, *125*, 73.
(75) Chia, V. K. F.; White, J. H.; Soriaga, M. P.; Hubbard, A. T. *J. Electroanal. Chem. Interfacial Electrochem.* **1987**, *217*, 121.
(76) Batina, N.; Frank, D. G.; Laguren-Davidson, L.; Lin, C. S.; Lu, F.; Salaita, G. N.; Stern, D. A.; Tarlov, M.; Walton, N.; Wellner, E.; Zapien, D. C.; Hubbard, A. T. *Anal. Chem.*, submitted.